# MEASUREMENT OF FLUID FLOW USING THE ULTRASOUND TIME DOMAIN CORRELATION TECHNIQUE IN A FLOW PHANTOM AND IN GUINEA PIGS

BY

AMJAD ALI SAFVI

B.S., University of Illinois at Urbana-Champaign, 1990
M.D., University of Illinois at Chicago, 1994

THESIS

Submitted in partial fulfillment of the requirements
for the degree of Master of Science in Electrical Engineering
in the Graduate College of the
University of Illinois at Urbana-Champaign, 1996

Urbana, Illinois

UNIVERSITY OF ILLINOIS AT URBANA-CHAMPAIGN

THE GRADUATE COLLEGE

JUNE 1996

WE HEREBY RECOMMEND THAT THE THESIS BY

AMJAD ALI SAFVI

ENTITLED MEASUREMENT OF FLUID FLOW USING THE ULTRASOUND TIME DOMAIN CORRELATION TECHNIQUE IN A FLOW PHANTOM AND IN GUINEA PIGS

BE ACCEPTED IN PARTIAL FULFILLMENT OF THE REQUIREMENTS FOR THE DEGREE OF MASTER OF SCIENCE

W. O'Brien

Director of Thesis Research

N. Narayana Rao

Head of Department

Committee on Final Examination†

Chairperson

† Required for doctor's degree but not for master's.

O-517

## ABSTRACT

Measurement of blood flow is an important consideration in diseases that involve the circulatory system. Ultrasound has been used extensively to measure blood flow in the past. There are two techniques that can be used to measure flow, Doppler and time domain correlation. In this thesis the time domain correlation technique is used. A computer implementation of the technique is developed. It is first verified by using it to calculate velocity from a known set of data. It is then used to measure controlled motion to verify its ability to track an object. A fluid flow phantom is developed in which a known rate of flow can be established. The phantom is utilized in the measurement of flow using the correlation technique. It is further tested in a live guinea pig to measure blood flow in various organs. The results verify the correct implementation of the time domain correlation technique. The phantom measurements confirm its ability to measure fluid flow. The guinea pig results do not confirm or deny the ability of the technique to measure flow in the live animal. It requires further examination and evaluation in the live animal model to determine its true capability to measure flow in complex flow patterns such as the micro- vasculature.

# DEDICATION

I would like to dedicate this thesis to my new baby, Zainab Fatima Safvi. She is a year old and I would like to tell her when she grows up how much I love her. I hope that she grows up to be a kind, pious, and God fearing human being. Her upbringing is foremost in my thoughts and I pray that she will follow the straight path in life, inshaallah.

ACKNOWLEDGMENTS

I would like to gratefully acknowledge the support and encouragement from my advisor, Professor William D. O'Brien, Jr. I would also like to acknowledge his guidance and patience in this work and for providing me with funding in the first year and helping me obtain the American Heart Association Fellowship last year. I truly appreciate his kindness and efforts in regards to my education.

I also would like to acknowledge the financial support of the American Heart Association in the form of a fellowship for the 1995-1996 school year to carry on this work.

I would finally like to acknowledge my wife's support and patience. Without her support it would have been impossible for me to finish the work. I appreciate her patience and am sorry for all the hardships she went through because of the long distances.

TABLE OF CONTENTS

LIST OF FIGURES

# CHAPTER 1

# INTRODUCTION

The measurement of blood flow through various tissues in the human body is of vital importance in some disease states such as constriction of coronary arteries in heart disease or of narrowing of carotid arteries, which could result in stroke. Ultrasound techniques have been developed over the years that measure flow in blood vessels that can help diagnose these conditions. There are two general ultrasonic techniques, Doppler and time domain correlation, which can be used to measure flow. The Doppler has been extensively studied and developed into clinical ultrasound systems that can determine blood flow in human blood vessels. Even though it is widely available, it has a major drawback in that it is unable to give very accurate quantitative results. The second technique, ultrasound time domain correlation (UTDC), overcomes this problem and has several advantages over the Doppler approach. This thesis presents the utilization of the UTDC technique to measure fluid flow in a flow phantom and its extension to measurements in a live guinea pig.

## 1.1 Doppler Technique

The Doppler technique is the most common technique used to measure blood flow. It uses the same principle as used in the Doppler radar in weather predictions or that of police radar. It measures a frequency change in the returned signal as a beam of ultrasound reflects off a moving target. The fundamental Doppler equation is

$$v = \frac{f_d c}{2 f_t \cos(\theta)} \tag{1}$$

where $v$ is the velocity of the moving target, $f_d$ is the Doppler shift (received frequency minus the transmitted frequency), $c$ is the speed of sound in the medium, $f_t$ is the frequency

of the transmitted signal, and $\theta$ is the angle between the sound beam and the axis of blood flow.

There are two types of Doppler devices, continuous wave Doppler and pulsed Doppler. The continuous wave (CW) Doppler uses a transmitting transducer, which puts out a continuous ultrasound wave that passes through the target and is picked up on the other side by a second transducer. This technique is unable to obtain velocity vs. range (distance) information since the range of the moving target is unknown because the wave is continuous.

In pulsed Doppler, one transducer sends out a time-limited pulse of ultrasound, which can be detected similarly to the CW case or its reflection can be detected by the same transducer after being reflected. In this case, since the transmitted wave is a pulse, range information is available. Since it is a short pulse, the signal is broad banded and suffers from the frequency-dependent attenuation effects described in the next section.

In both of the Doppler cases, the Doppler angle and the blood vessel diameter are unknowns making a quantitative measure of blood flow impossible.

### 1.1.1 Disadvantages of Doppler technique

One of the disadvantages of the Doppler technique is that the Doppler shift is never a single frequency but a band of frequencies [1]. The velocity must be estimated from the mean frequency.

Another major disadvantage is the frequency-dependent attenuation of tissues. This effect can be modeled as [2]

$$A(f) = A_0 f^b \tag{2}$$

where $A(f)$ is the total attenuation as a function of frequency, $A_o$ and $b$ are frequency-independent tissue constants, and $f$ is the frequency in megahertz. This leads to different attenuations for different frequencies in the same tissue.

Another frequency-dependent effect is due to backscattering of ultrasound from moving red blood cells that are smaller than a wavelength. They are considered to be Rayleigh scatterers and scatter power which is proportional to the fourth power of the frequency. As a result, higher frequencies scatter more power than lower frequencies. Because these frequency-dependent effects are unpredictable from patient to patient, the Doppler can not give a quantitative measure of flow.

## 1.2 Ultrasound Time Domain Correlation (UTDC) Technique

The correlation technique differs from the Doppler technique in that it does not measure a frequency shift but a shift in time of two consecutive waves. It tracks an echo in time and finds the velocity of the scatterers by correlating two consecutive echoes.

Briefly, a pulse of ultrasound is directed towards a group of moving scatterers and a characteristic reflection depending on the group of scatterers is returned to the transducer. A time $\Delta t$ later another pulse at the same frequency (from the same transducer) is sent to the same location. The scatterers have moved a distance $\Delta d$ in that time period. The second echo contains the same characteristic reflection which has moved within the second echo a certain distance when compared to the first echo. The amount of distance the characteristic reflection has moved in the second echo when compared to that for the first echo is indicative of the velocity of the scatterers. This shift can be converted to a velocity if the pulse repetition frequency (PRF) and the angle between the ultrasound beam and the flow direction are known. The amount of shift is found by calculating the location of the highest correlation coefficient of the two consecutive echoes.

### 1.2.1 Advantages of UTDC

The correlation technique in effect estimates the change in position of the scatterers in a certain time as opposed to estimating a change in frequency as in the Doppler technique. This leads to certain advantages for the correlation technique. The moving scatterers can be tracked in time [3] as opposed to the Doppler where no tracking is possible. Also the scatterers do not have to be in motion at the time of data acquisition in order to estimate the motion [3]. This leads to application of the correlation technique for other situations than velocity estimation. For example, the correlation technique can be used to track a tissue as it is compressed to yield various tissue properties, such as the bulk modulus.

## 1.3 Comparison of UTDC and Doppler Techniques

### 1.3.1 Precision

Precision is a measure of the repeatability of a measurement and can be defined as the standard deviation of the measurements divided by the mean of the measurements. Thus a smaller number for precision is desirable. Embree [4] and Embree and O'Brien [5] have previously calculated both theoretically and experimentally the precision of UTDC and Doppler techniques. The raw unfiltered precision has been reported to be 5 to 10% [4],[5] for UTDC. An estimate of the raw Doppler precision has been made by Embree [4] to be in the range of 86 to 124%. Bassini et al. [6] have analyzed the theoretical variance of the Doppler and UTDC techniques and have found that both perform similarly for signal to noise ratios (SNR) greater than 10. For SNRs of less than 10, UTDC works significantly better.

As the scatterers move laterally through the beam, the correlation coefficient declines. If the distance that the scatterers move within the PRF time period is small, the

correlation coefficient is high and vice versa. Foster et al. [7] have shown that the correlation coefficient decreases linearly as the amount of lateral motion increases and that the precision of UTDC is dependent on the amount of translation within the beam. In UTDC, therefore, the maximum measurable velocity is best stated in terms of precision. The theoretical precision for the system described by Foster et al. is shown in Figure 1.

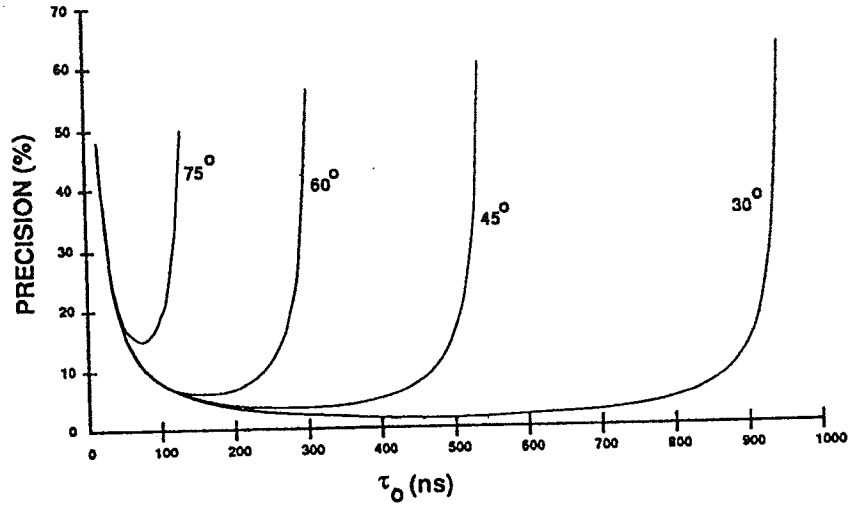


Figure 1. Theoretical precision versus time shift and measurement angle (from Foster et al. [7]).

### 1.3.2 Aliasing

The Nyquist criterion, which limits the detection of the maximum Doppler frequency, states that the sampling rate has to be at least twice the highest frequency to avoid aliasing. In the case of Doppler if the moving blood produces Doppler shifts that exceed the Nyquist criterion, aliasing occurs and high velocities appear as low velocities. Therefore, in Doppler, aliasing limits the highest detectable frequency.

In the case of UTDC, aliasing does not affect the measurements, and the maximum measurable velocity is limited by the PRF and the beam width. The scatterers can only be tracked while they are in the beam and the PRF determines how much time the scatterers can stay in the beam. Therefore, with a high PRF, the scatterers can move faster and still be

tracked within the beam but if the PRF is low the scatterers will have moved out of the beam and no tracking is possible.

### 1.3.3 Bandwidth vs. resolution

The bandwidth of the transmitted pulse affects the precision of both the UTDC and Doppler. In the case of UTDC, a higher bandwidth (shorter pulse) results in better spatial resolution. In the case of Doppler, the lower the bandwidth (longer pulse), the better the precision. Therefore, when working with either technique, a compromise has to be made between axial resolution and precision.

### 1.3.4 Frequency dependence of intervening tissues

There are two different frequency-dependent effects. The intervening tissues affect the received signal in the Doppler and distort it according to the equation $A = A_o f^b$ as mentioned previously in Section 1.1.1. Also the blood cells act as Rayleigh scatterers and scatter power proportionally to the fourth power of the frequency. Doppler suffers from both effects and produces biased results.

In contrast, UTDC does not suffer from such biasing because all the echoes pass through the same intervening tissues of a patient and therefore produce accurate flow velocities for different patients with different intervening tissues. This has been analyzed further by Embree and O'Brien [2] and Ferrara et al.[8].

### 1.3.5 Direction determination

The UTDC technique is such that the direction of flow can be found from the time shift without having to construct additional hardware to compare the incoming signal with a reference signal as is the case in Doppler. The direction naturally falls out when the time shift is determined.

## 1.4 Thesis Outline

Chapter 2 further develops the UTDC technique and explains the derivation in greater detail. The second half of Chapter 2 describes an implementation of the UTDC technique in Matlab and further explains how the various parameters in the program affect the results. Chapter 3 describes the testing of the program. It is divided into two sections, one dealing with testing the program with simulated data and the other dealing with testing the program with collected data. Chapter 4 explains the fluid flow phantom and how measurements are made. It presents the results from several completed experiments which explore the relationships among the various parameters affecting the measurements. Chapter 5 describes how the measurements in the guinea pigs are done and presents the results including some ultrasound images made in the live guinea pig. Chapter 6 contains the conclusion.

CHAPTER 2

# ULTRASOUND TIME DOMAIN CORRELATION TECHNIQUE AND ITS IMPLEMENTATION

This chapter covers the theory and concept of the UTDC technique and presents its development . In the second half of the chapter a computer implementation is presented.

## 2.1 UTDC Technique

### 2.1.1 Continuous time derivation

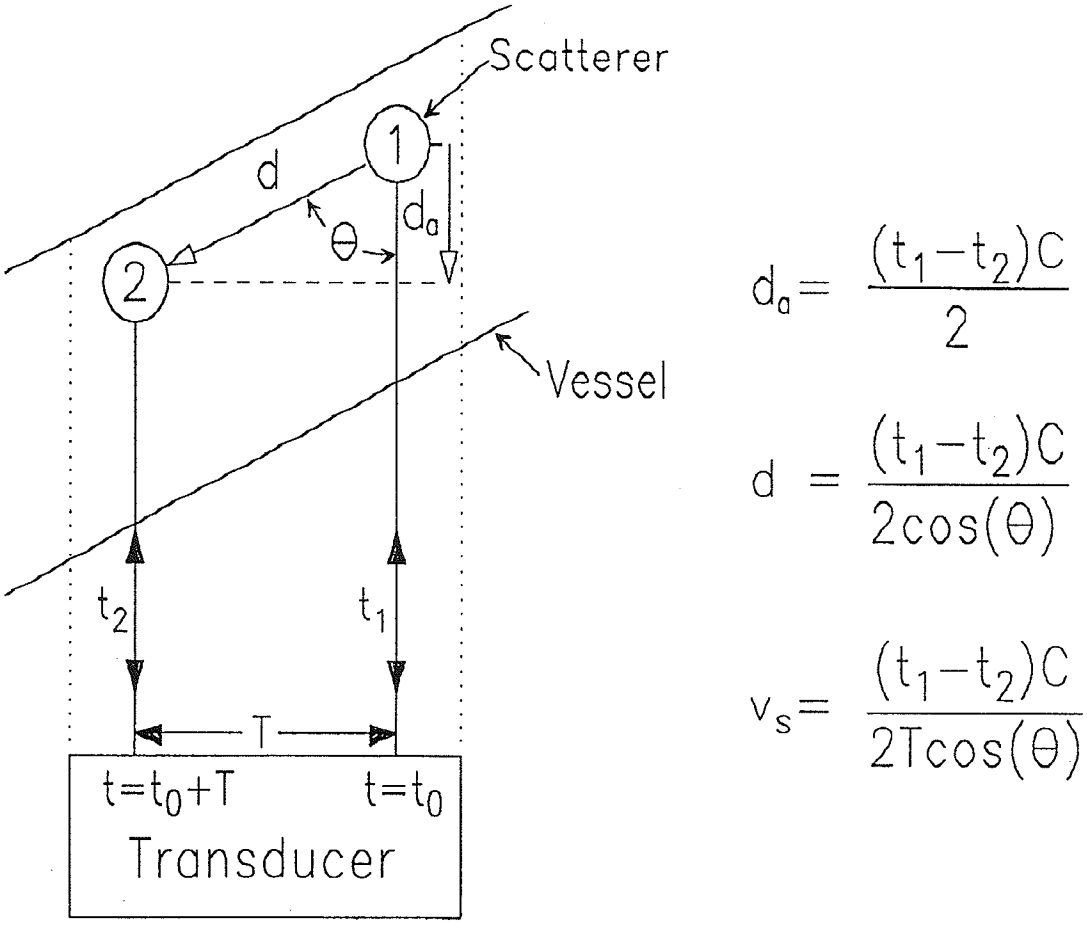


Figure 2. Ultrasound time domain flowmeter concept (from I. A. Hein [1]).

The UTDC concept is illustrated in Figure 2. A transducer produces an ultrasound pulse which is scattered at location 1 and receives the echo from the scatterers in a vessel at location 1. The round trip takes time $t_1$. The vessel is at an angle $\theta$ from the transducer. A time $T$ later the same group of scatterers moves an unknown distance d from their original location at 1 to a new location at 2 along the vessel. A second pulse is produced a time $T$ later and returns a second echo from location 2, and this second echo takes a round trip time $t_2$. The aim is to find the velocity from this information. The difference of the two round trip echo times $t_1$ and $t_2$ can be determined. The distance $d_a$ can be calculated from

$$d_a = \frac{(t_1 - t_2)c}{2} \tag{3}$$

where $t_1$ and $t_2$ are the round trip echo times and $c$ is the speed of sound in the medium between the transducer and the vessel. The factor of 2 is in the denominator because $t_1$ and $t_2$ are round trip times. After $d_a$ is known, $d$ can be simply calculated by using the definition of cosine

$$d = \frac{d_a}{T} = \frac{(t_1 - t_2)c}{2\cos(\theta)} \tag{4}$$

where$T$ is a known time quantity and the velocity becomes

$$v = \frac{d}{T} = \frac{(t_1 - t_2)c}{2T\cos(\theta)} \tag{5}$$

In this equation, $\theta$ is known as the Doppler angle or the measurement angle. The change in time $t_1 - t_2$ is known as the time shift or $\tau$ and is analogous to the frequency shift in the Doppler technique. All the quantities are known except the time shift, which is estimated by using correlation. The angle $\theta$ is a known quantity in the experiments done to measure flow, although in clinical situations $\theta$ can be calculated from the B-mode image. It is also possible to determine the $\theta$ without prior knowledge by sweeping an ultrasound beam

across the vessel and forming profiles of constant flow which results in an elliptical shape. Several($M$) ellipses are calculated. The minor and the major axes from each ellipse can be used to calculate the angle as done in [5] according to

$$\theta_M = \frac{1}{M}\sum_{n=0}^{M-1}\sin^{-1}\left[\frac{a_n}{b_n}\right] \tag{6}$$

where $a_n$ is the half minor axes length and $b_n$ is the half major axis length of the $n$th constant velocity ellipse.

In a tube there is a group of scatterers instead of a single scatterer. This group of scatterers which in three dimensions occupies a volume gives the echo and the characteristic signal. Figure 3 shows a group of scatterers as it moves across the ultrasound beam in a vessel.

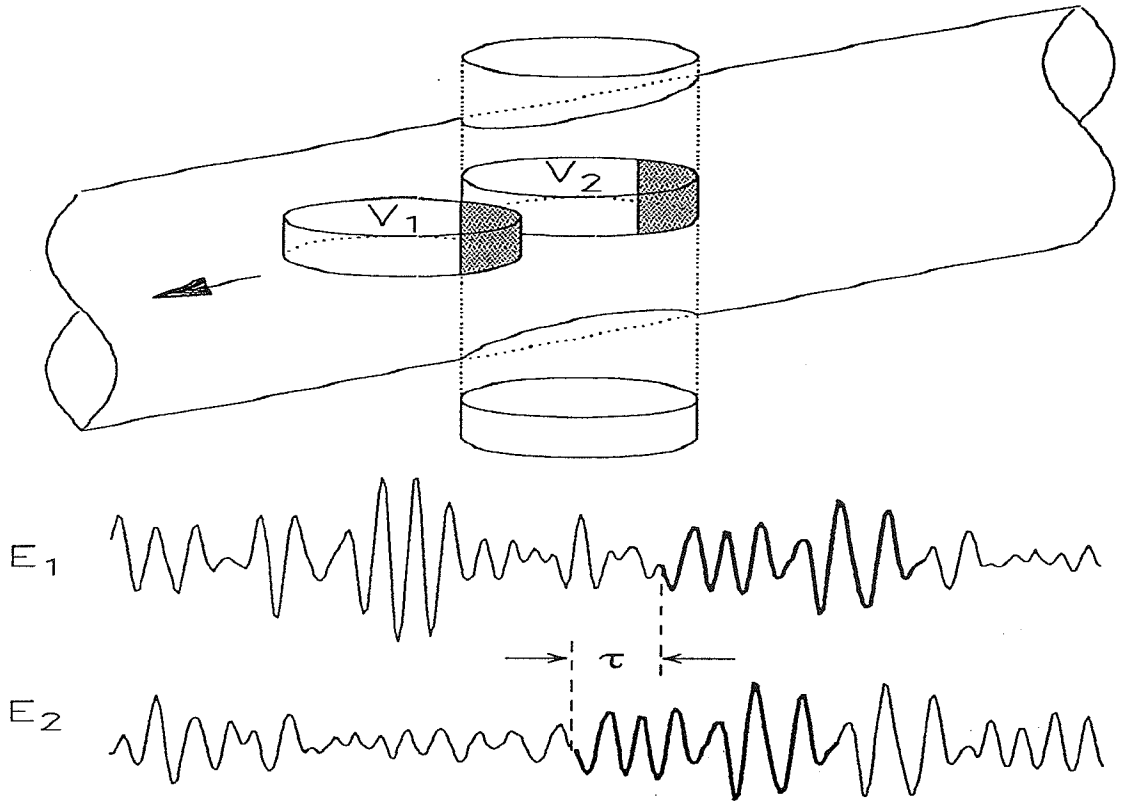


Figure 3. Shift of the ultrasound signal as scatterers move down the tube. The actual ultrasonic echoes are due to all scatterers within the ultrasonic beam. $E_1$ is the echo due to volume 1 which has moved out of the beam. $E_2$ is the echo due to volume 2, still within the beam. The common sections of $V_1$ and $V_2$ will produce similar sections of echo in $E_1$ and $E_2$ (from I. A. Hein [1]).

$V_2$ represents the volume at $t_1$ which shows the characteristic echo shown as $E_2$. A time $T$ later the volume shown as $V_1$ has moved down the vessel and a portion of the volume left inside the beam. That portion is also shown in $V_2$ as a darkened area. The characteristic echo from $V_1$ is given by $E_1$. The darkened portions of the volumes $V_1$ and $V_2$, which is the same group of scatterers remaining within the beam, are represented by the darkened waveforms in $E_1$ and $E_2$. The darkened waveforms are exactly the same because they are echoes from the same group of scatterers. The waveform other than the darkened portion changes as the volume changes within the beam. The darkened waveform stays the same within the larger waveform and shifts by an amount $\tau$ as the group of scatterers move down the vessel. The time shift $\tau$, from which the velocity can be calculated, is the missing piece of information that has to be determined.

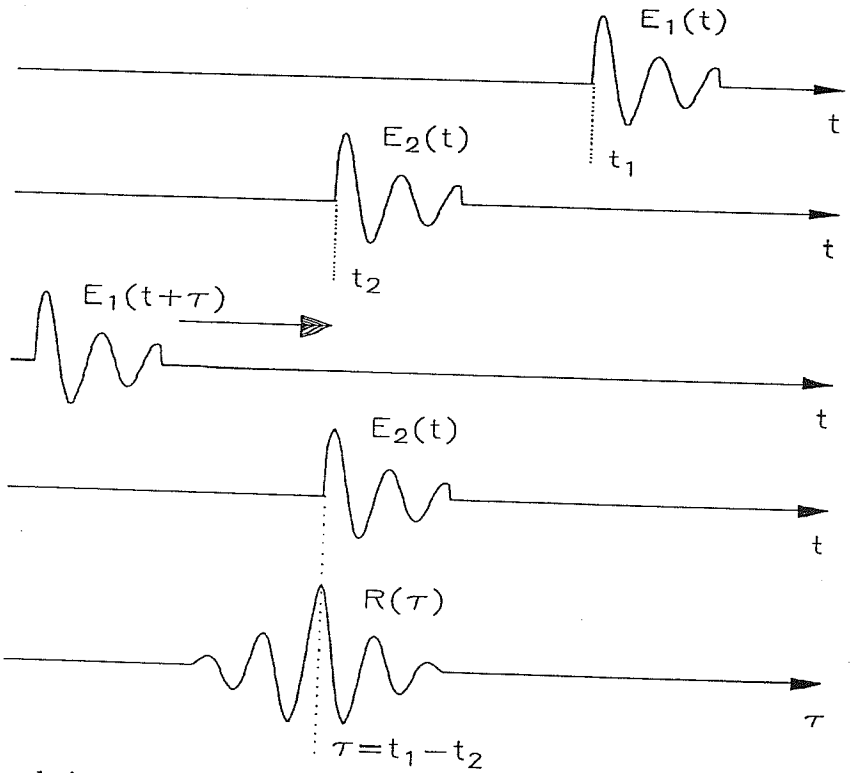


Figure 4. The correlation of two echoes consists of shifting one echo back in time by $\tau$ and multiplying it by the other to produce the correlation coefficient $R(\tau)$. The value of $\tau$ producing a maximum $R(\tau)$ corresponds to $\tau = t_1 - t_2$ (from I. A. Hein [1]).

Correlation can be used to determine $\tau$. This is done in order to find the location of the best match of two waveforms, one at $t_1$ and the second a time $T$ later at $t_2$. The concept is illustrated in Figure 4. If there are two similar waveforms, $E_1(t)$ and $E_2(t)$ , where $E_1(t)$ starts at $t_1$ and $E_2(t)$ starts at $t_2$, the correlation is done by shifting one waveform back in time by $\tau$ and sliding it along the second waveform. This is similar to convolution except in correlation a multiplication is done instead of an integration according to

$$R(\tau) = \sum_t E_1[t+\tau]E_2[t] \tag{7}$$

As the first wave slides across the second wave the two waves are multiplied to compute a correlation coefficient $R(\tau)$. The largest value of the correlation coefficient will be at a point when the similar waveforms overlap exactly. This peak will occur at a value of $\tau$ which represents the difference between $t_1$ and $t_2$. The correlation coefficient is usually normalized to unity by dividing it by the square root of the product of the squares of the two waves. The normalized correlation coefficient is

$$R(\tau) = \frac{\sum_t E_1[t+\tau]E_2[t]}{\sqrt{\sum_t [E_1(t+\tau)]^2 \sum_t E_2[(t)]^2}} \tag{8}$$

2.1.2 Discrete time derivation

In Figure 5 there are two digitized waveforms, $E_1(n)$ and $E_2(n)$, with a section within each waveform being exactly the same (boxed portion). A section of the first waveform $N$ points long starting at $t_1$ and $r$ points from the beginning is boxed out and shifted across the second wave. It is correlated with a portion of the second wave also $N$ points long producing a correlation coefficient curve as a function of $s$, where $s$ is the location of points within the box. $R(s)$ will show the maximum value which is 1 at an $s$ value of $\tau$. $\tau$ is the time shift $t_1 - t_2$ and the correlation coefficient is 1 if the boxed wave

exactly matches a portion of the second wave. The normalized digitized correlation coefficient is given by

$$R(s) = \frac{\sum_{i=0}^{N-1} E_1[r+i]E_2[r+i+s]}{\sqrt{\sum_{j=0}^{N-1}[E_1(r+j)]^2 \sum_{k=0}^{N-1}[E_2(r+k+s)]^2}} \tag{9}$$

and produces a value between 1 and -1, where 1 represents a perfect match, 0 represents completely dissimilar waves, and -1 represents two completely inverted waves.

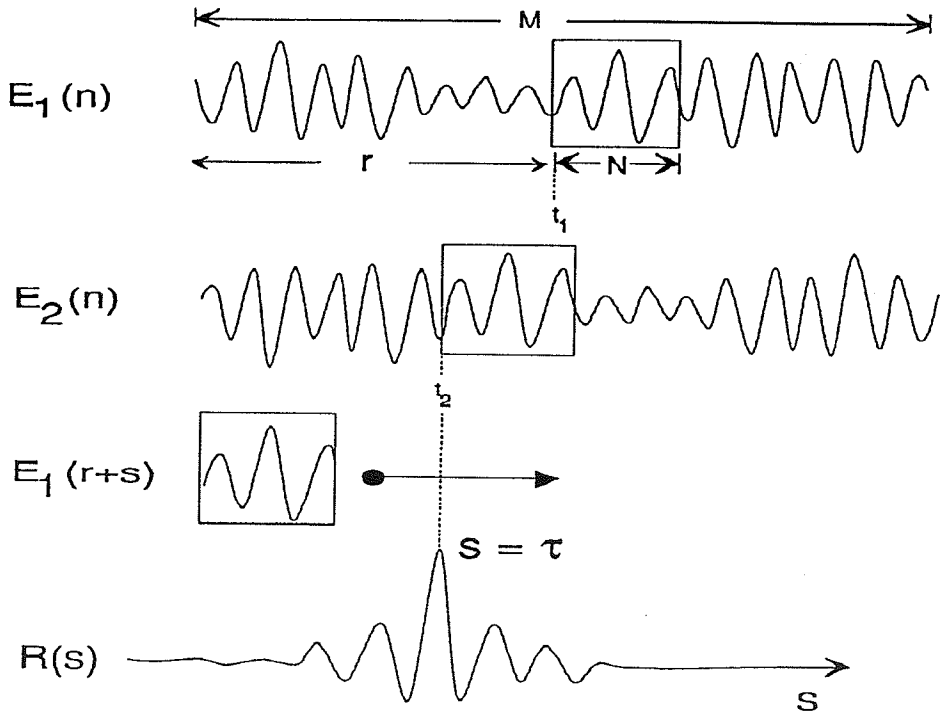


Figure 5. The correlation of two digitized echoes consists of windowing out a desired section of one echo and correlating it at different locations $s$ along the other echo. The value of $s$ producing maximum $R(s)$ corresponds to $s = \tau$ (from I. A. Hein [1]).

Selecting the value of $s$ where there is a maximum value of $R$ gives the time shift needed to calculate the velocity. The time shift value in seconds can be calculated by multiplying the shift in pixel value, $s$, with the A/D sampling rate given in seconds/pixel. Regions along the wave can be sampled individually to give velocities corresponding to different ranges from the transducer. A plot of velocity versus range can then be constructed to give a one-dimensional flow profile across the vessel diameter as shown in Figure 6.

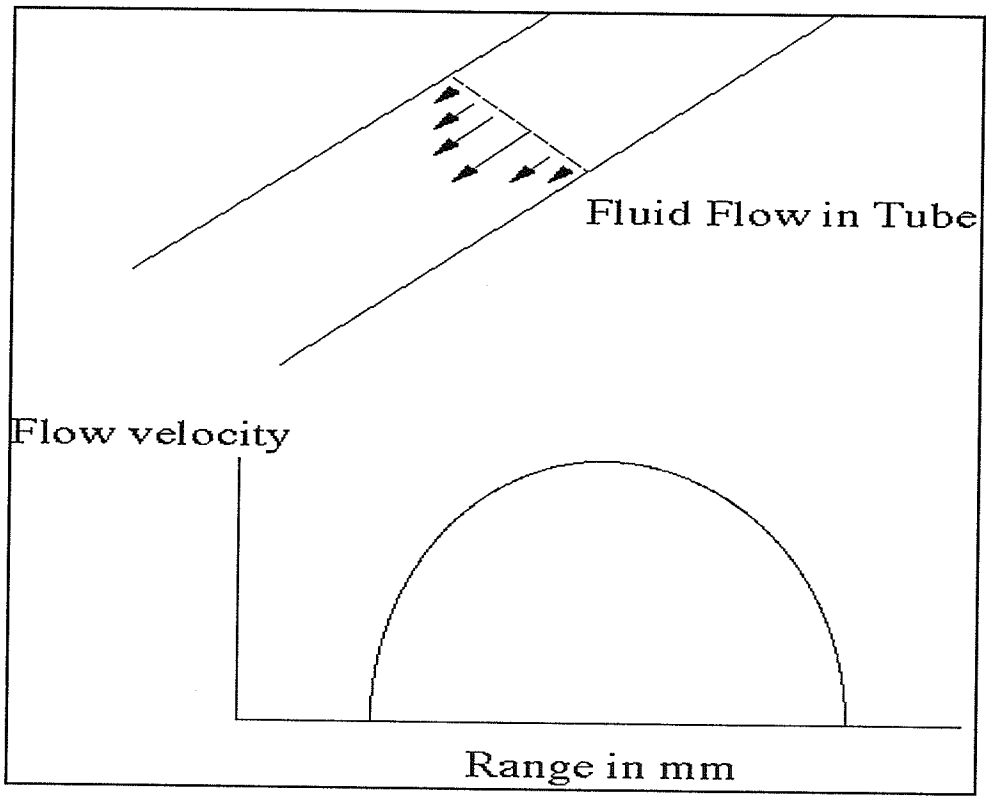


Figure 6. Fluid flow shown in one dimension in a tube. The flow is laminar with a parabolic shape. The bottom graph depicts a one-dimensional velocity profile across the tube.

## 2.2 Computer Implementation

The UTDC technique has been implemented in Matlab and the algorithm will be explained in this section. The Matlab code implements the UTDC technique to plot one-dimensional velocity versus range profiles obtained by a focused single-element transducer.

It requires several parameters, which are changed for any new set of experimental conditions, to find velocity. These include the sampling rate, number of points in a wave, the measurement angle, and PRF. There are several options within the program that can be selected to run it differently for each set of data. These include the number of waves that will be correlated with each other, a variable to decrease PRF if desired, a variable to limit the correlation search area to a region of interest, an option to control range resolution, and a variable to control the resolution of how closely the correlations are done.

### 2.2.1 Correlation algorithm

#### 2.2.1.1 Acquisition of data

The Matlab program starts by reading in a binary data set which is acquired by a LeCroy 9354 TM digital oscilloscope. The LeCroy scope stores the data in its flash memory and later the data are transferred to a 486PC computer over a GPIB connection. The data are arranged in a one-dimensional array since each wave acquired is appended to the previous wave. The number of waves acquired can be controlled by the scope. The data are then transferred to a Unix workstation where they can be read and analyzed by the correlation program to yield one-dimensional velocity versus range profiles.

#### 2.2.1.2 Overview of algorithm

Briefly, the data are parsed into separate waves in a two-dimensional array so that individual waves can be manipulated. Each wave is subdivided into a number of adjacent sections (input variable), the more the sections the greater the range resolution. Each section is then correlated to the next wave in a predetermined region of interest of the next wave to see where the best match occurs. The next wave is also divided into same length sections differing in location by 1 pixel. The center index of the original section is compared with the center index of the section of the next wave which produces the highest

correlation coefficient. The difference in the center indices gives the $\tau$ in pixels which can be multiplied by the sampling rate to yield the time shift in seconds.

2.2.1.3 Description of result figures

After the program has separated the input data file into individual successive waves, it opens several figures in Matlab to display the results. In Figure 1 Matlab displays the individual waves. In Figure 2 Matlab displays the velocity profiles, each being generated from a comparison of two adjacent waves. Figure 3 in Matlab displays the maximum correlation coefficient for each section (aggregate correlation curve) for the two adjacent waves. Figure 4 in Matlab displays the correlation curves from which the aggregate correlation curve is generated. Figure 5 in Matlab displays a single velocity profile after averaging all the individual velocity profiles in Figure 2 of Matlab.

2.2.1.4 Limiting the search area

After Figure 1 in Matlab is opened, the first wave is plotted. Then a calculation is made to limit the correlation search area with the input variable maxsearchvel, which represents the maximum flow that will be encountered when making the flow measurements. Since the PRF of the transducer can be set and, therefore, is known as well as the measurement angle and the sampling rate, and if a maximum flow rate is chosen, the maximum number of pixels that two adjacent waves are allowed to be shifted under these conditions can be solved for from the velocity formula (Equation (5)). This formula can be restated as

$$v(\text{cm/s}) = \frac{(\text{number of search pixels})(\text{sampling rate})(\text{speed of sound in the medium})}{2(\text{time period between two waves})\cos(\theta)}$$

This formula can be used to solve for the number of search pixels since all the other variables in the equation are known. This reduces the computation time considerably because it limits the search to usually tens of pixels, the amount of actual shift, instead of a thousand or more pixels, i.e., the number of pixels in one wave.

2.2.1.5 Main loop

After making this calculation, the main loop is started which correlates two adjacent waveforms. The first step in the loop divides the first wave into a number of sections (input variable) as shown in Figure 7. Then it picks the next wave and plots it adjacent to the first wave in figure 1 of Matlab. The first iteration of the main loop is reserved to do a correlation between the first wave and itself. This step is included as a rough check on the correlation algorithm to see if it is working properly. A comparison of exactly the same waves should give a zero shift in pixels or a zero value for $\tau$ for the time shift resulting in a zero velocity. Consequently, the first velocity profile in figure 2 of Matlab which results from a correlation of the first wave with itself should be a flat line at zero.

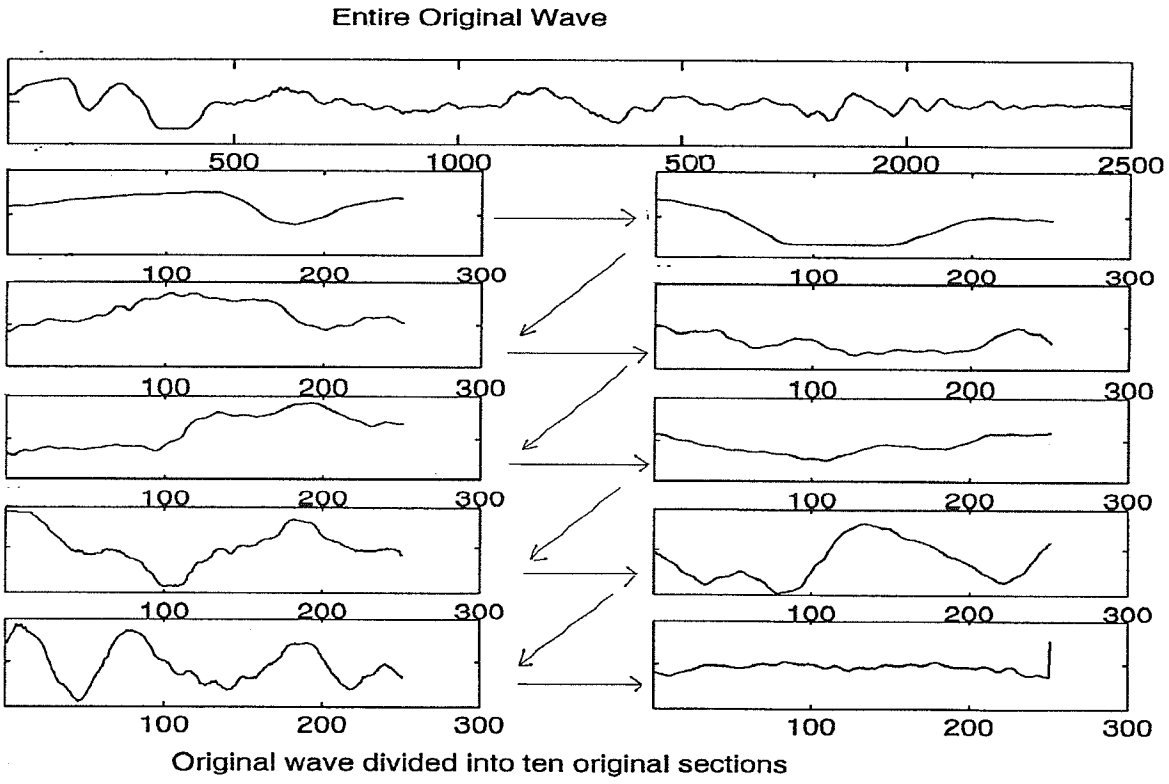


Figure 7. One wave divided into ten adjacent sections. The entire wave is shown on the top. The lower graphs each show 1/10th of the wave in the order depicted by the arrows.

The main loop divides the second wave into sections that are not adjacent as in the first wave but sections that are moved by one pixel from the previous section as seen in Figure 8. These new sections are the same length as the original sections from the first wave. For the new sections, having the same length is necessary because the Matlab function for correlation, xcorr, requires two waves of the same length. This step of dividing the second wave into many new sections (number of new sections=number of points in one wave-length of one section) is a very time-consuming and memory-consuming step since a very large array has to be created to store the new sections (size of new section array=(number of points in one wave-length of 1 section)xlength of one section).

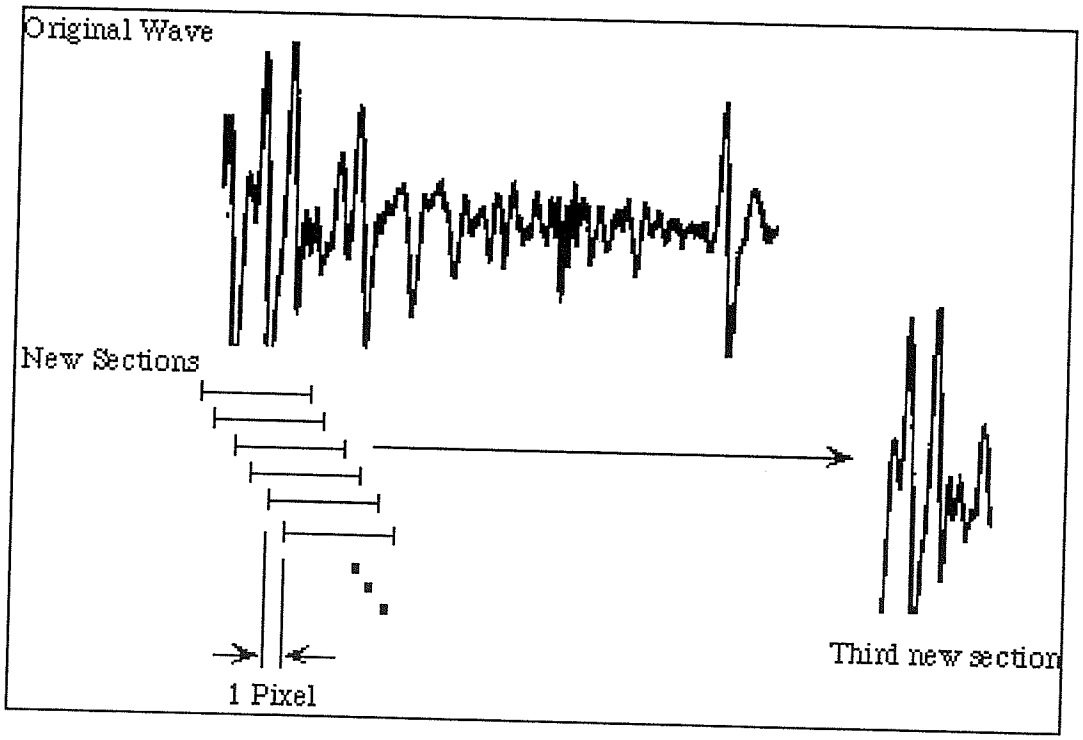


Figure 8. One wave shown divided into new sections. Each new section is shifted by one pixel and is the same length as every other new section.

A subloop in the main loop correlates each of the original sections with new sections around the location of the original section, the search area being limited by the maxsearchvel input variable. The subloop returns a correlation curve for each correlation

done between the original section from the first wave and several new sections from the second wave. The subloop picks the maximum correlation value from each correlation curve done between the original section and the numerous new sections and creates a new curve containing the maximum correlation coefficients from all of the individual correlation curves. This "aggregate" curve contains the information to calculate the $\tau$. The maximum of this aggregate curve is located where the best match occurs, and after comparing the center index of the original section with the index of the location of the maximum gives the time shift in pixels which can be converted to a time shift as described earlier ( Figure 9).

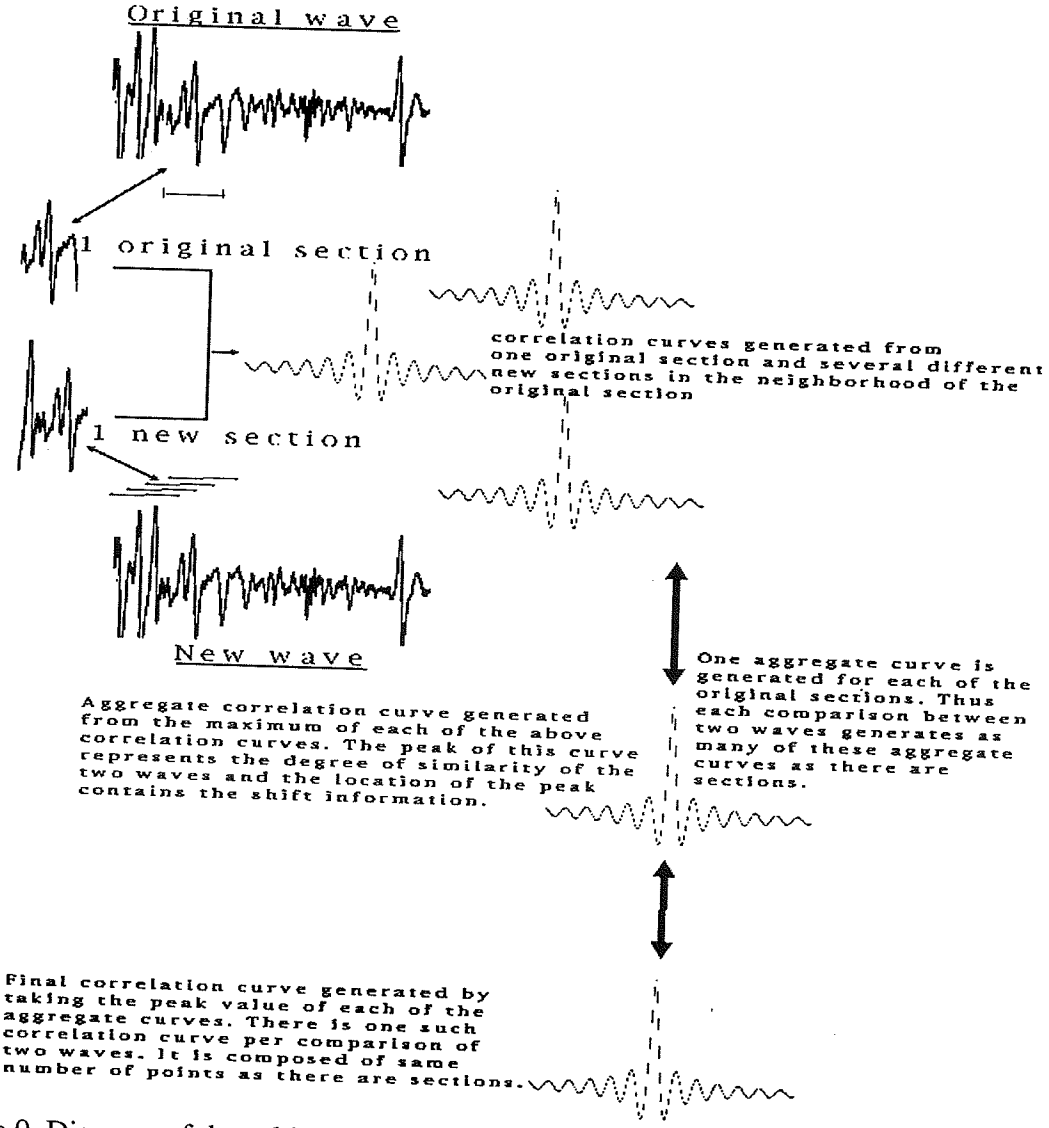


Figure 9. Diagram of the subloop explaining how the final correlation curves are generated.

Figure 2 in Matlab plots the velocity versus section number (range) after calculating the velocity from Equation (5). As mentioned previously the first velocity profile should be zero since two exact waves are correlated. Each of the following profiles in the figure is generated by comparing two succeeding adjacent waves.

Figure 3 in Matlab contains the plots of the maximum correlation coefficient found for each section. This maximum is the maximum of the aggregate correlation curve which represents one original section. This final correlation curve is a measure of the similarity of the two adjacent waves. If the correlation coefficients are near one, then the program was able to track the scatterers well. If the correlation coefficients are low, then the scatterers were moving too fast or PRF was too low due to the inability of the program to track the targets well. Another possibility of having low correlation coefficients may be that the scatterers did not maintain their shape as they moved within the ultrasound beam leading to decorrelation of two adjacent waves. This effect can be due to not maintaining laminar flow which will be considered later in Chapter 4.

Figure 4 in Matlab plots the aggregate curves for each section of the first wave and figure 5 in Matlab plots the average of the individual velocity profiles generated in figure 2 of Matlab. As a last step the program saves the figures as well as the velocity and the correlation data generated.

### 2.2.2 Effects of input parameters

#### 2.2.2.1 Effect of corr_resolution

The input variable corr_resolution determines how closely the correlations are done, i.e., how many new sections are skipped between each correlation done with the original section. The new sections differ from each other by 1 pixel. The corr_resolution determines those new sections of the original sections to which it will correlated. If corr_resolution is 1, then the original section will be correlated with every new section within the area of interest defined by maxsearchvel. This is the highest resolution that can be achieved to

generate an aggregate curve. If corr_resolution is set to 2, then the loop will skip every other new section for the correlation between the original section and the new sections. This leads to less computation time (time is halved since only half as many correlations are done) but the accuracy in determining the time shift is sacrificed, i.e., the resolution of the time shift, $\tau$, is halved. If the corr_resolution is set to 3, the computation time is reduced to 1/3 of the original time but the time shift resolution is decreased by 3. The best value to pick for corr_resolution is 1 since at the flow rates measured, the time shift is only in the tens of pixels.

This fact was a major impediment in the development of this program. In the beginning it was assumed that the shift would be in the hundreds of pixels. This led to great frustration due to the fact that two adjacent waves would not be correlated to any great extent. The original sections would correlate with the wrong new sections since the correlations were done by skipping many new sections where there was a better match. This led to complete decorrelation and useless results. The best approach was to set corr_resolution to 1 at the expense of computation time to gain greater time shift resolution. The computation time can be reduced greatly by limiting the search area with the input variable maxsearchvel.

#### 2.2.2.2 Effect of maxsearchvel

The input variable maxsearchvel puts a limit on the region of the second wave where the correlations are done. This is done so that unnecessary computations are not done. As stated previously the maxsearchvel is converted to the number of pixels. The search is done starting that many number of pixels to the left and the same amount of pixels to the right of the original section (see Figure 10). This saves considerably the computation time compared to when there is no limit on the search area. Without a limit the original section would be correlated to the entire second wave which can take a factor of ten to a hundred times more to complete the computations.

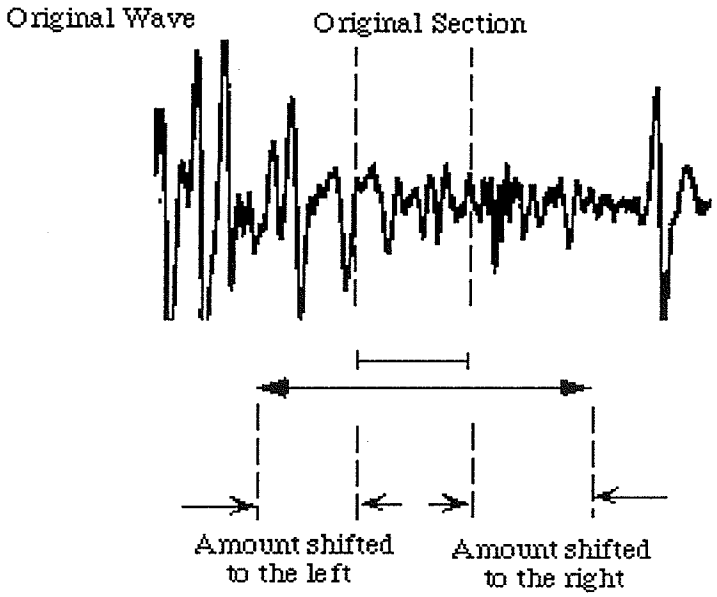


Figure 10. Limits on the distance searched on either side of the original section.

2.2.2.3 Effect of radtheta

The measurement angle, theta, is the angle between the transducer and the tube. As this angle approaches 90 degrees, the axial velocity component (the component of the flow in the direction of the ultrasound beam) becomes zero. Therefore a small angle is desired to increase the axial component of velocity. If the angle is small, the scatterers stay in the ultrasound beam for a longer time period. This reduces the demand to have a faster PRF because the time between two waves can be longer before scatterers move out of the beam. Also the time shift $\tau$ is greater since the scatterers move for a greater distance in the axial direction while staying in the beam. If the angle is close to 90°, the time shift will be smaller and harder to detect and the flow rates will have to be reduced or PRF will have to be increased to keep the scatterers within the beam.

2.2.2.4 Effect of everykthscan

The input variable everykthscan determines which waves are correlated. If it is set to 1, two adjacent waves will be compared. If it is set to 2, the loop will skip one wave and

correlate every other wave and similarly for a value of 3 it will skip 2 waves. This variable can decrease the effective PRF by a factor of the integer value chosen for everykthscan. It can not increase the PRF since that is determined by the Panametrics pulser/receiver. This variable was included so that measurements can be made at the highest PRF and an appropriate PRF can be chosen for the flow rate without having to worry about too low a PRF. The highest PRF available with the Panametrics pulser/receiver is 10 kHz giving a T (period) value of 100 μs.

There is an upper bound on how fast a PRF can be used in an experimental setup. The faster the PRF the less time there is available for a pulse to be sent and received before the next one is started. If a second pulse is sent while the first one is returning, both pulses can interfere with each other in the medium. Thus a second pulse has to wait for the first one to return before it can be sent. If this time is reduced, it decreases the amount of distance the first pulse can be allowed to travel because longer distances take more time to cover. This can place a limit on how far the sample is placed or how much of the sample can be measured. At the flow rates measured, this was not a major concern because 10 kHz was a fast enough PRF.

#### 2.2.2.5 Effect of pointsin1wave

The number of points in a single wave can be chosen by the LeCroy scope. The best compromise between having a better spatial resolution (large number of points) and less computational requirements (less points) was between 1000-2000 points per wave. The LeCroy scope gives a choice of having 500, 1000, 2000, 2500, or 5000 points in that range. It does not let the user choose an arbitrary number of points. If 5000 points are chosen to increase spatial resolution or to cover a longer spatial area, the memory requirements to create the new section array far exceed any benefit accrued from having better spatial resolution. In fact looking at just one 5000-point wave can take several hours to create the new section array. This is a drawback to the program and better ways of

implementing the search algorithm have not been explored. Therefore waves consisting of 1000 or 2000 points are preferred.

2.2.2.6 Effect of timebetweenwaves

This input variable is the period, *T,* in the velocity formula and is determined by the PRF chosen on the pulser/receiver. The highest PRF (10 kHz) is desired but in some situations it can be too high. For example if the flow is very slow, a slower PRF is desired to get a large enough time shift between two waves. If the PRF is high in slow flow conditions, the two adjacent waves may essentially be the same and not give a large enough $\tau$ that can be measured. Using everykthscan to reduce the effective PRF can help but this increases the requirement to capture more waves. This increases the size of data files. Therefore an appropriate PRF should be chosen for the flow conditions to minimize unnecessary data collection.

2.2.2.7 Effect of timeperpointus

This variable is the A/D sampling rate of the scope. It determines the spatial resolution of the ultrasound measurement. If it is high more points per wave are acquired, which increases the spatial resolution at the expense of a larger computation time. The A/D sampling rates available with the LeCroy scope far exceed the requirements for flow measurements. An added benefit of having a high sampling rate (1 GHz) is noise reduction in the signal. The signals from the LeCroy scope are much less noisy than from the older Tektronix scope.

2.2.2.8 Effect of sections

The number of sections determines how many pieces the first wave will be divided into. If it is a large number, a greater range resolution can be achieved at the expense of having to do more correlations.

# CHAPTER 3

# VERIFICATION OF PROGRAM

To validate that the correlation program worked, two situations were created where the data set could be verified to contain a measurable time shift. In the first case an actual echo was taken from a data set (a single A-line) and artificially shifted by a predetermined amount to generate successive waves. This newly created data set was fed to the correlation program to see if it gave a uniform velocity. In the second case a uniform target was moved towards and away from the transducer (angle=0) to see if the program could track the target.

## 3.1 Creation of a Wrapped Wave

A single A-line consisting of 2500 points was separated from a data set captured from a flow experiment. A portion of the wave from the left side consisting of 100 points was removed and added to the right side of the wave after shifting the original wave by 100 points to the left. This generated a second wave. This second wave in effect shifted the original wave by 100 points to the left and cut off the 100 points that moved left and added them to the other side of the wave. Similarly subsequent waves were generated from previous waves.

These new waves contain a constant shift of 100 pixels between two waves and this shift is present throughout the whole wave since the entire wave is shifted by the same amount. If the wave is divided into sections, the program should show that all the sections shift by a similar constant amount. This would lead to a constant velocity profile. If the program produces such results, then we can be reasonably certain that it is performing in a correct manner.

The program was run with $\theta$ and $T$ set to an arbitrary value. This can be done because there is no real value for a velocity that depends on $\theta$ and $T$ and the only interesting result is the shape of the velocity profile. In this case there is no motion of any kind and the data are artificially generated.

Figure 11 shows the artificially created waves. The first wave in the top left corner represents the original A-line captured from a flow experiment. As stated in the last chapter the wave is duplicated in the top right corner to check for the validity of further calculations. This initial step should always give a zero velocity profile since there is no shift. In Figure 11 and similar figures that display waves and results, the progression of subsequent waves is from the top left to the right, then the lower row of figures from left to right and so on. In this figure there are six separate waves shown each shifted by 100 points to the left, top two being the same wave.

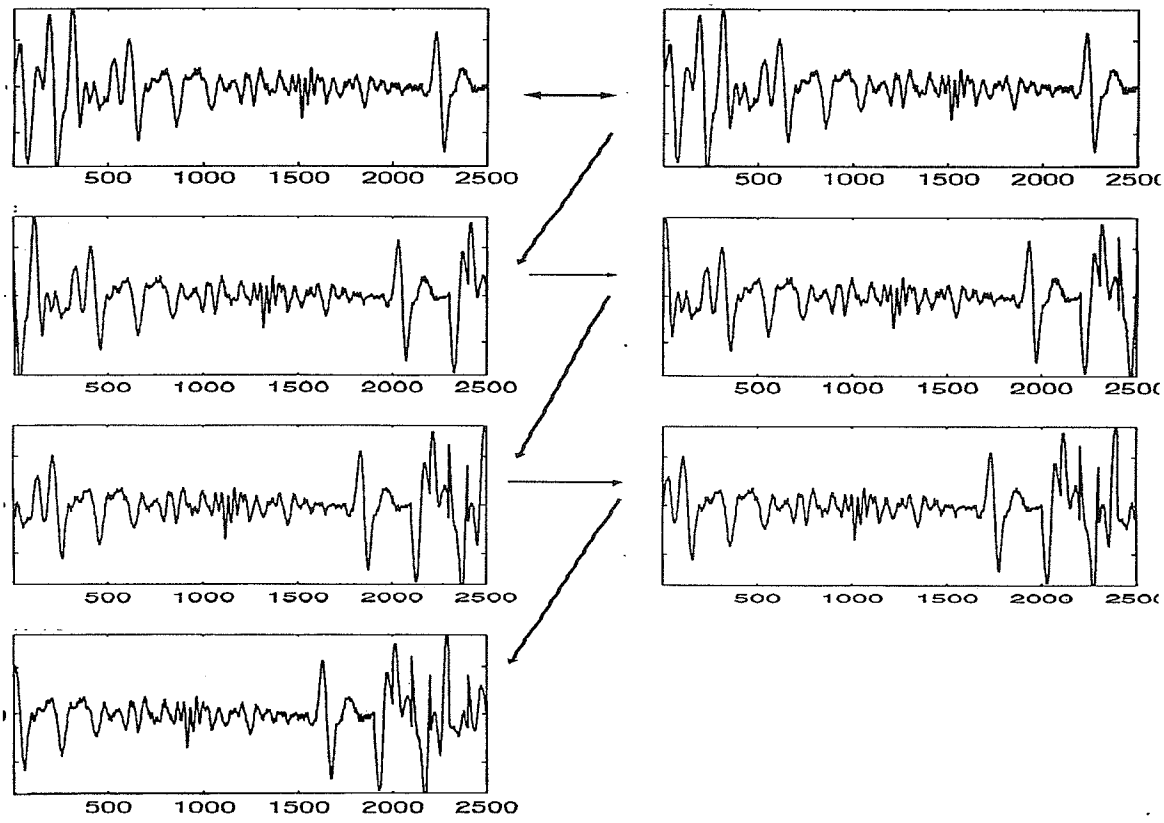


Figure 11. A wave wrapped around itself. Each new wave is generated by shifting the old one by a hundred points to the left.

## 3.2 Wrapped Wave Correlation Results

### 3.2.1 Wrapped wave results without sectioning the wave

Figure 12 shows the velocity results of the correlation program and Figure 13 shows the corresponding correlation curves. In the top left corner is the velocity profile generated from comparing the first two waves in Figure 11. As expected, the velocity profile is a line at zero. The y-axis scale is in arbitrary units and does not represent a flow rate since this is artificial data which does not represent a measured flow. The x axis represents the number of sections into which the wave was divided. In this case it was 10. The top right figure represents a comparison between the first and the second waves and shows that the velocity calculated is constant and positive. If the shift would have been in the other direction, the velocity would have given a negative value. Similarly, the subsequent graphs represent velocity profiles of two adjacent waves in the order mentioned above.

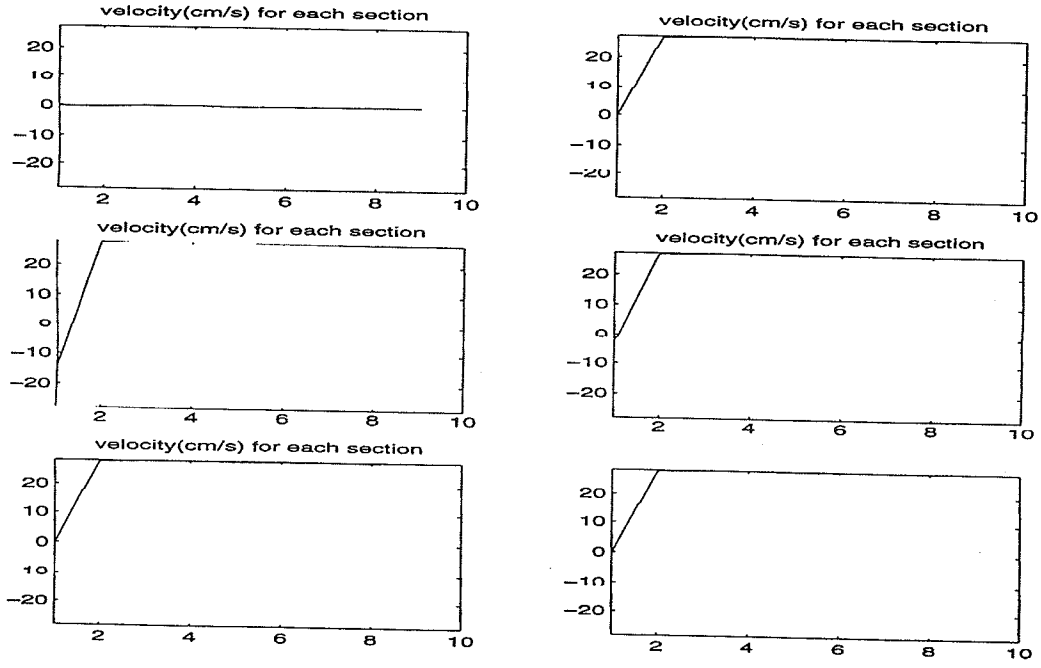


Figure 12. Velocity profiles for the wrapped wave. Y axis does not represent true velocity. X-axis is the section number.

The velocity in the figures starting with the second one is not entirely the same value but there is a region over section one that gives different values of flows. This can be explained by the fact that the search can be conducted to the right of the first section but not to the left of it since there are no points to the left of the first point. This shortcoming results in not being able to find a left shift in the area of the first section, and since it can only search in one direction it often gives the best correlation at the wrong location.

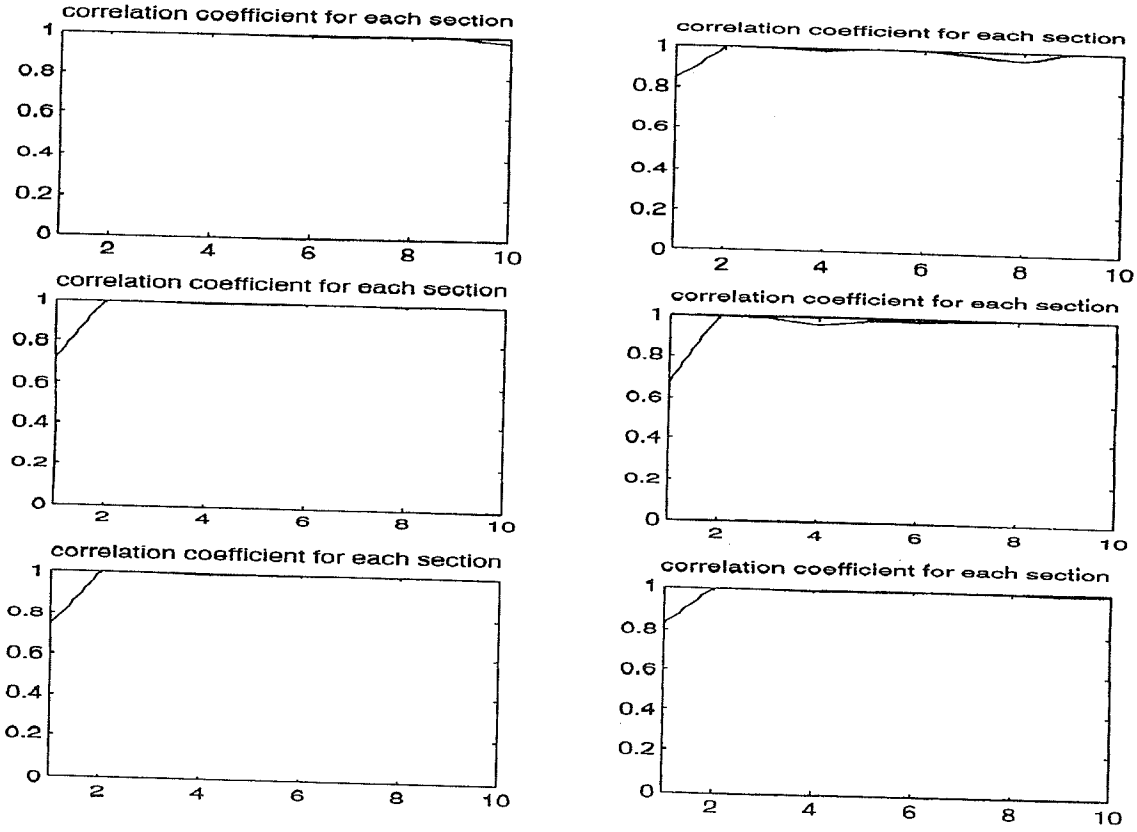


Figure 13. Final correlation curves for the wrapped wave data set.

### 3.2.2 Wrapped wave results with sectioning

In a similar simulation, the same data set was run with the correlation program with three shifted waves instead of six. This simulation compared the first wave with subsequent waves instead of comparing two adjacent waves. This demonstrates the ability of the program to determine variable shifts. Figure 14 shows the three waveforms, the first

two in the top row are the same, the bottom left is shifted by 100 points, and the bottom, right is shifted by 200 points. Figure 15 displays the results. In the top part of the figure, the first curve (top left) as expected is a zero velocity curve. The second has a "velocity" of 25 cm/s corresponding to a shift of 100 points, and the third has a "velocity" of 50 cm/s corresponding to a shift of 200 points. The third graph shows a velocity twice as much as the second since the shift is twice as much verifying the validity of the results. The bottom graph in Figure 15 shows the corresponding aggregate correlation curves. These also indicate a mismatch at section one by having a low correlation coefficient at that location.

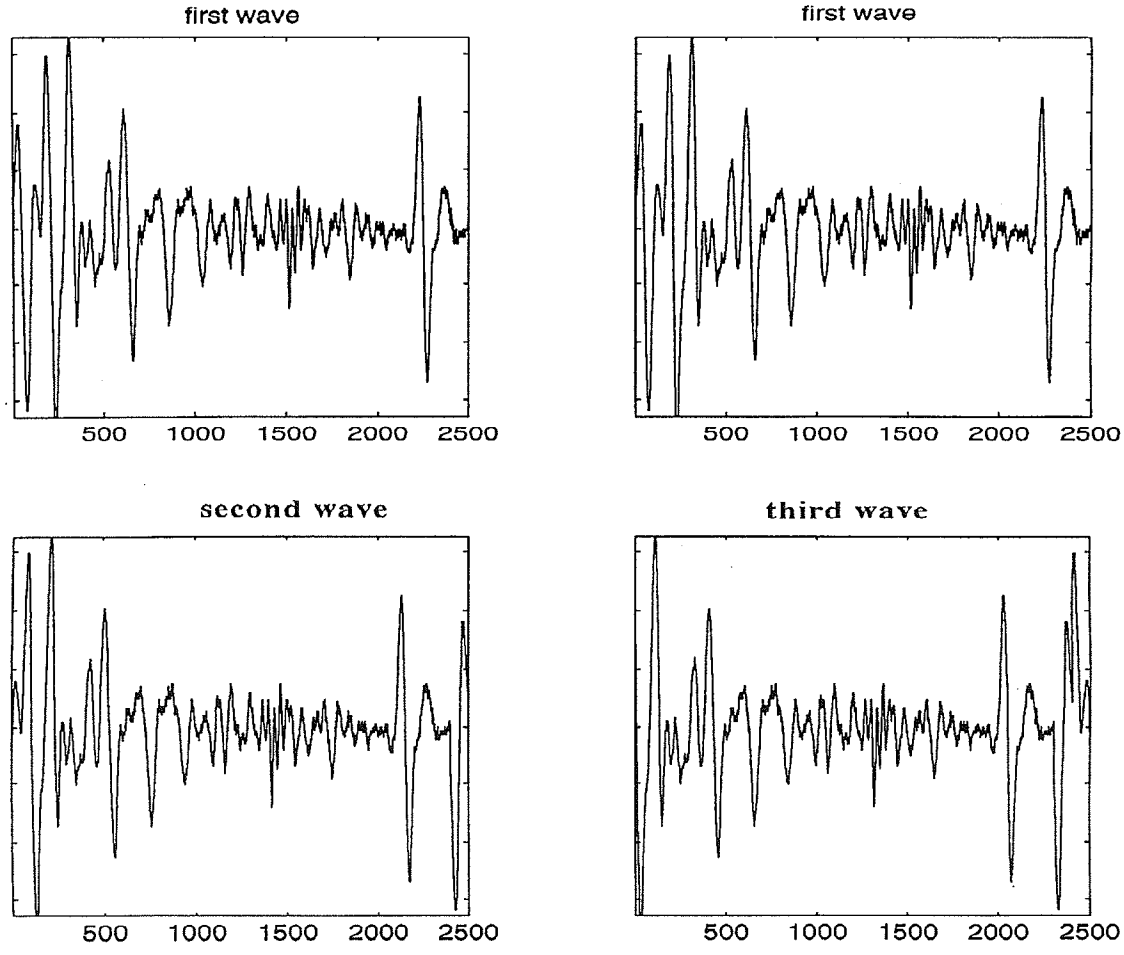


Figure 14. Three different consecutive waves from the wrapped wave data set.

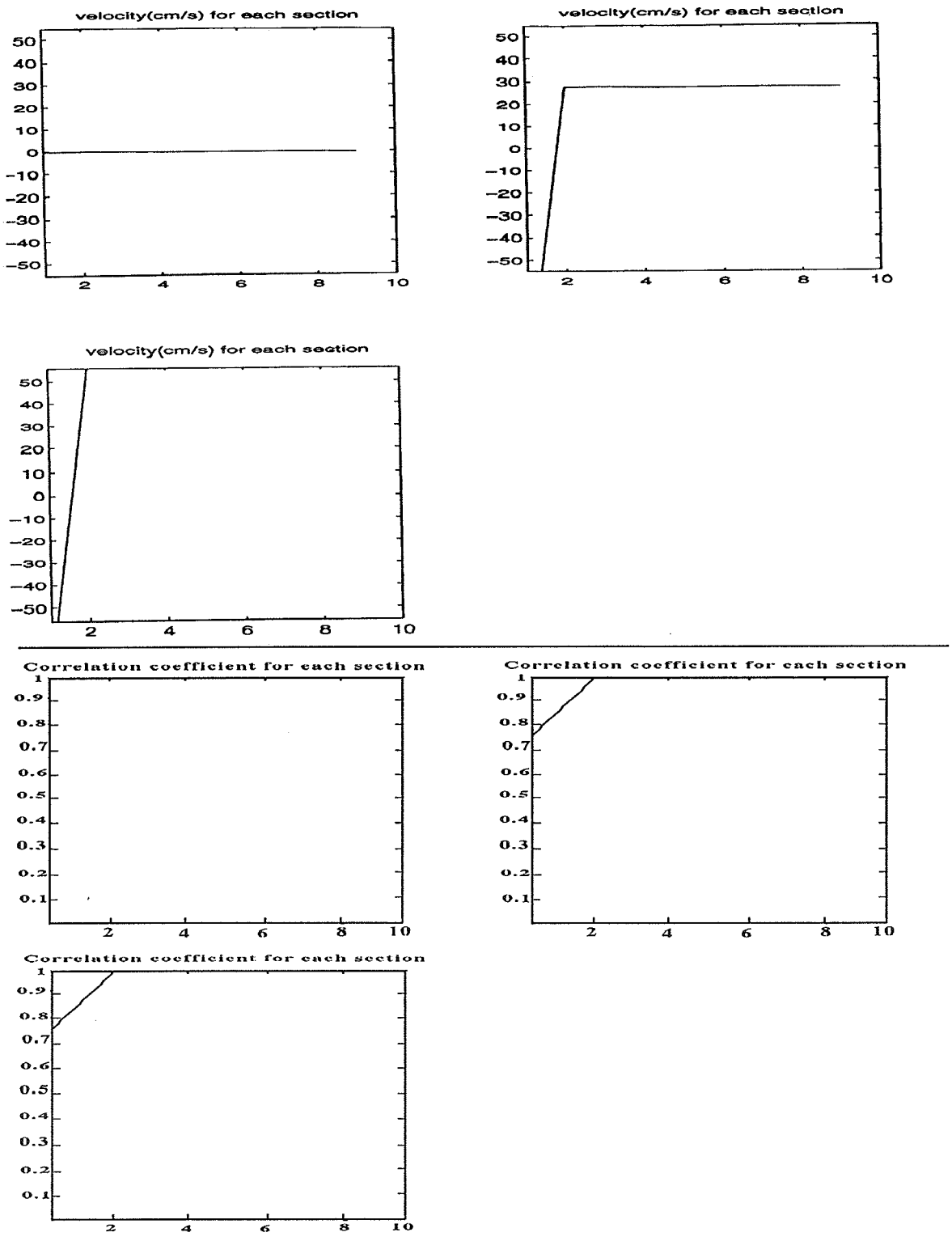


Figure 15. Velocity and correlation profiles for the wrapped wave. Top half: velocity profiles calculated by comparing the first wave with itself, first wave with the second, and first wave with the third. Bottom half: corresponding correlation curves.

## 3.3 Testing With a Moving Target

After the simulations verified that the program is able to find time shifts consistently, a moving target was chosen so that it could be tracked to see if time shifts could accurately be determined with actual collected data.

### 3.3.1 Data acquisition

Figure 16 shows the moving target.

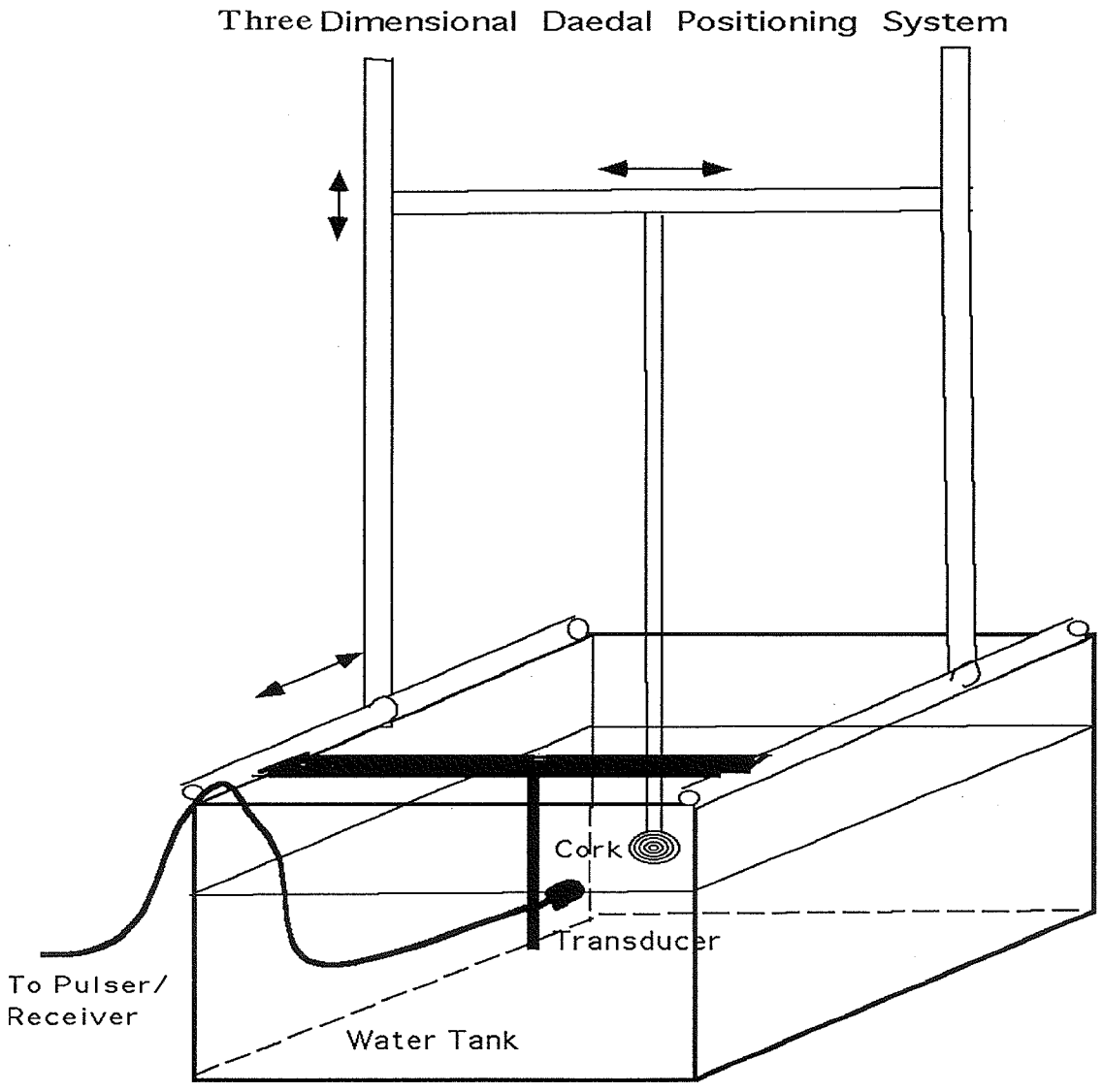


Figure 16. Three dimensional Daedal positioning system used in motion experiments.

A cork is used as a moving target while a Panametrics 5 MHz transducer is positioned such that the ultrasound beam hits the moving target. The cork is moved in the direction of the transducer with the aid of a Daedal 3-D positioning system capable of moving a point in space with an accuracy of 4 μm. In this experiment movement is in one dimension and towards the transducer. In the experiment the target moves a predetermined amount and then stops. The data are acquired while the target is stationary. The transducer is driven by a Panametrics 5800 pulser/receiver, and the received echoes from the transducer are monitored by a Tektronix 11401 oscilloscope. The scope is attached to a 486 PC computer via a GPIB connection which can collect the waveforms as well as drive the Daedal positioning system. The software to drive the Daedal system and collect data was written by Nadine Smith, Ph.D., from the Bioacoustics Laboratory.

### 3.3.2 Results

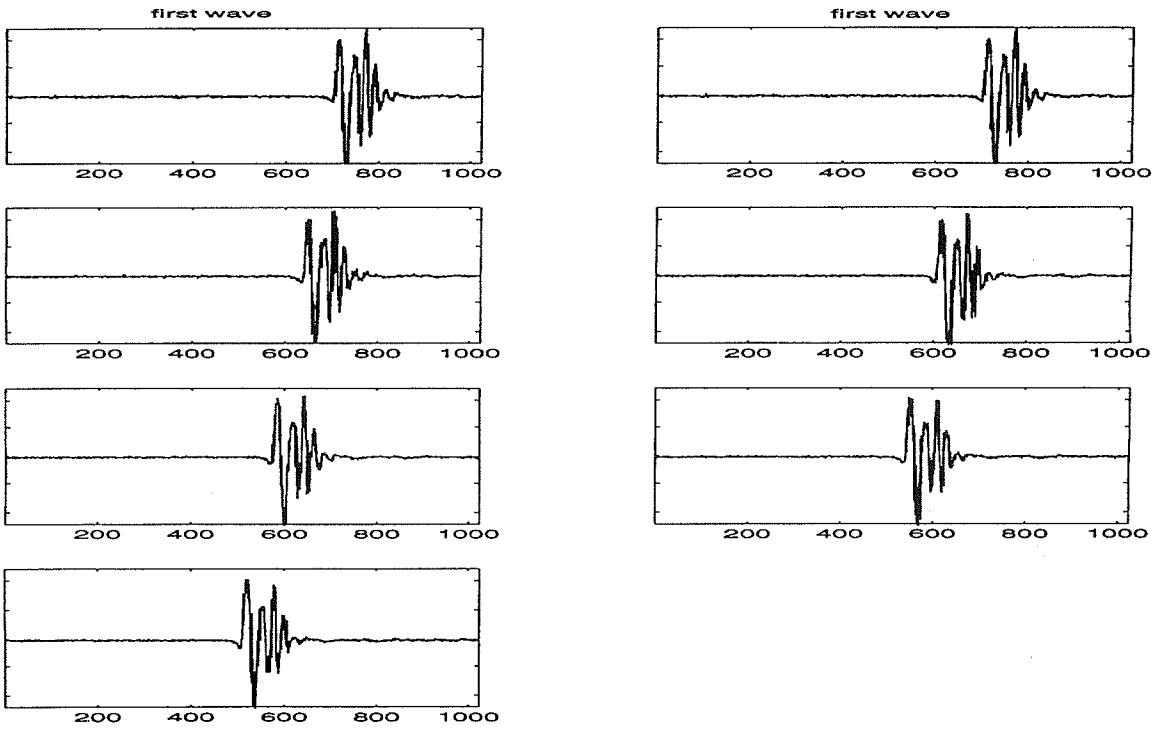


Figure 17. Ultrasound pulse/echo signal as the target moves towards the transducer.

Figure 17 shows six collected waves from one such experiment where the target (a circular piece of cork) is moving towards the transducer. As can be seen from the waves, the target creates a large echo signal some distance from the transducer which can be seen to be moving towards the transducer. The criterion for a successful run of the program is to see whether it gives a flat velocity profile since the movement is constant.

The program described in Chapter 2 was not used here but an earlier version of the program, which was much simpler, was used. The same general principles apply in this program. It uses the correlation function and finds the maximum correlation and its location but can not divide the wave into sections or calculate velocity in centimeters per second. In effect it correlates two entire waves. Since the target is not in true motion (it is stopped when the data are taken) no true velocity is measured. The result is only indicative of the amount of motion between waves and direction of motion.

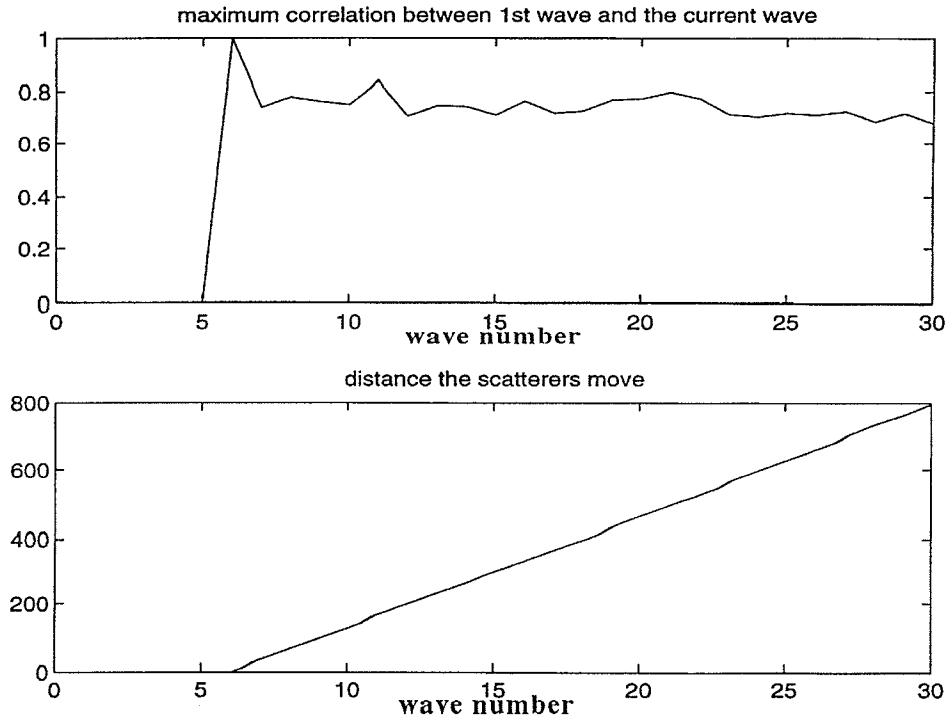


Figure 18. Correlation and displacement results from a motion experiment. The first wave is correlated with every subsequent wave.

In Figure 18, the first wave is correlated with the subsequent waves starting with the sixth one. The top curve is the correlation curve made from the maximum correlation values from two entire waves. The x axis represents the number of the wave. The first point in the correlation curve represents the maximum correlation value from the correlation between the first and the sixth waves. The next point similarly represents a correlation done between the first and the seventh waves and so on. The bottom curve represents the amount of shift that occurs for each comparison. This indicates a displacement but not velocity. As can be seen , the displacement between the first and the subsequent waves is increasing.

In Figure 19 the same program was used but the correlations were done between two adjacent waves. The correlations started from the 1st wave. The correlation curve looks similar but the displacement curve is flat indicating the shift between two adjacent waves is the same . This in fact is true since the target moved a constant amount before each wave was captured.

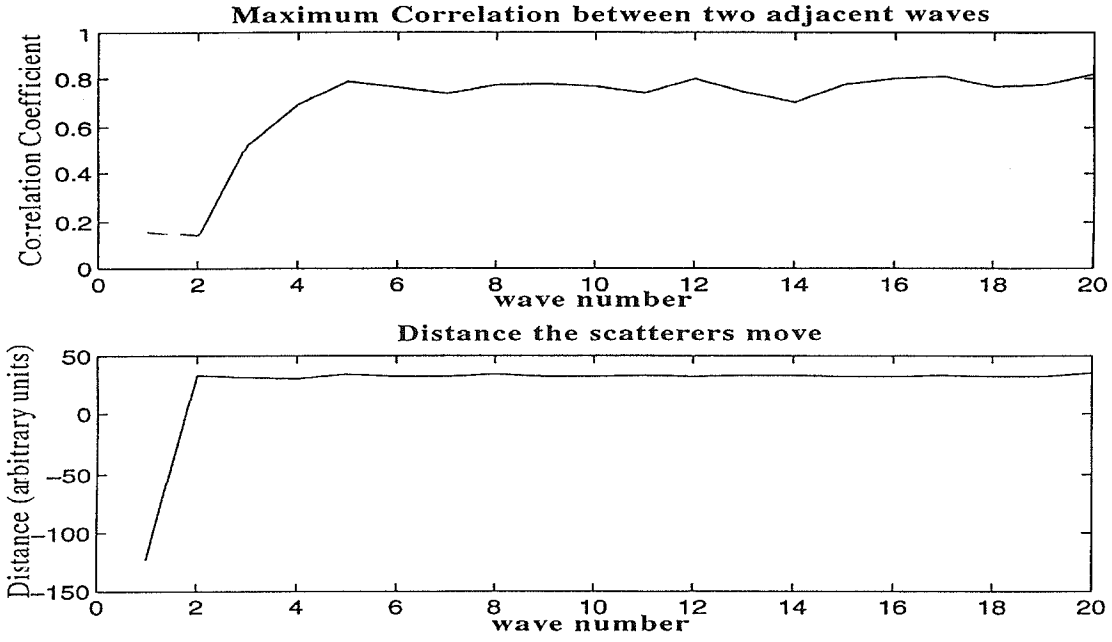


Figure 19. Correlation and displacement results from a motion experiment. Adjacent waves are correlated.

A different target, circular piece of soft plastic, was used to generate the results shown in Figure 20 by correlating the first wave with the subsequent waves. The left graph shows a movement of the target towards the transducer and the right graph shows a movement in the opposite direction indicating the capability of the correlation program to detect direction as well as motion. The amount of motion between two waves was greater when the cork was moving away from the transducer.

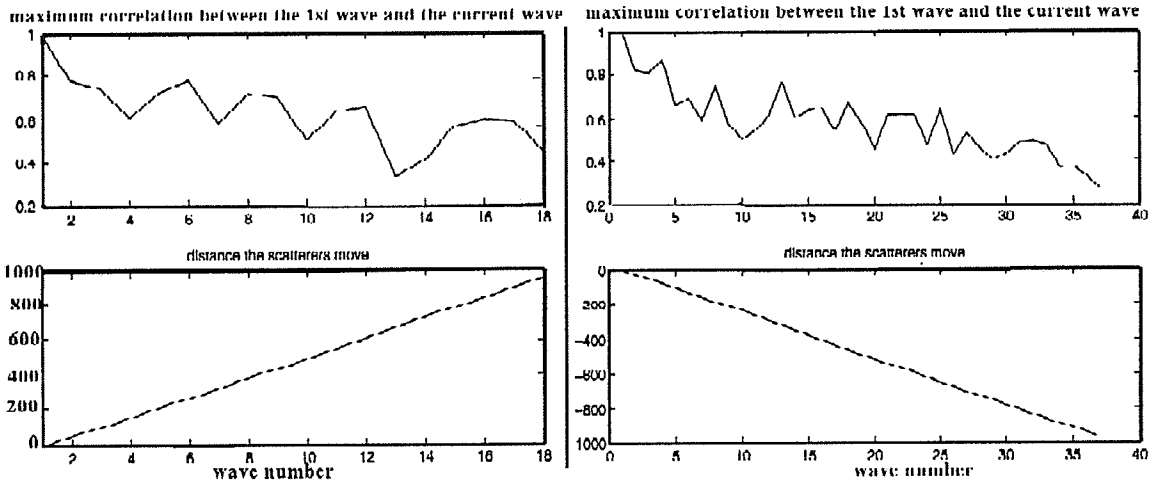


Figure 20. Correlation and displacement results from a motion experiment. The first wave is correlated with every subsequent wave. Two different directions of travel are compared. Y axis is correlation coefficient for top graphs and distance (arbitrart units) for bottom graphs.

The data shown in Figure 17 were also used in the final version of the program to see if the motion could be detected only in the right side of the waves since the signal always occurs in that region and stays within that region. The capability of the program to break up the waves into sections of the new program gives the ability to increase the range resolution. This was used to generate a motion rather than a velocity profile. All six of the waves were used. Each wave was broken into 20 sections, which is represented by the x axis. The top left part of Figure 21 shows the corresponding aggregate correlation curves.

Adjacent waves were correlated and the velocity results for each individual correlation between two adjacent waves are shown in the top right part of Figure 21. The bottom part

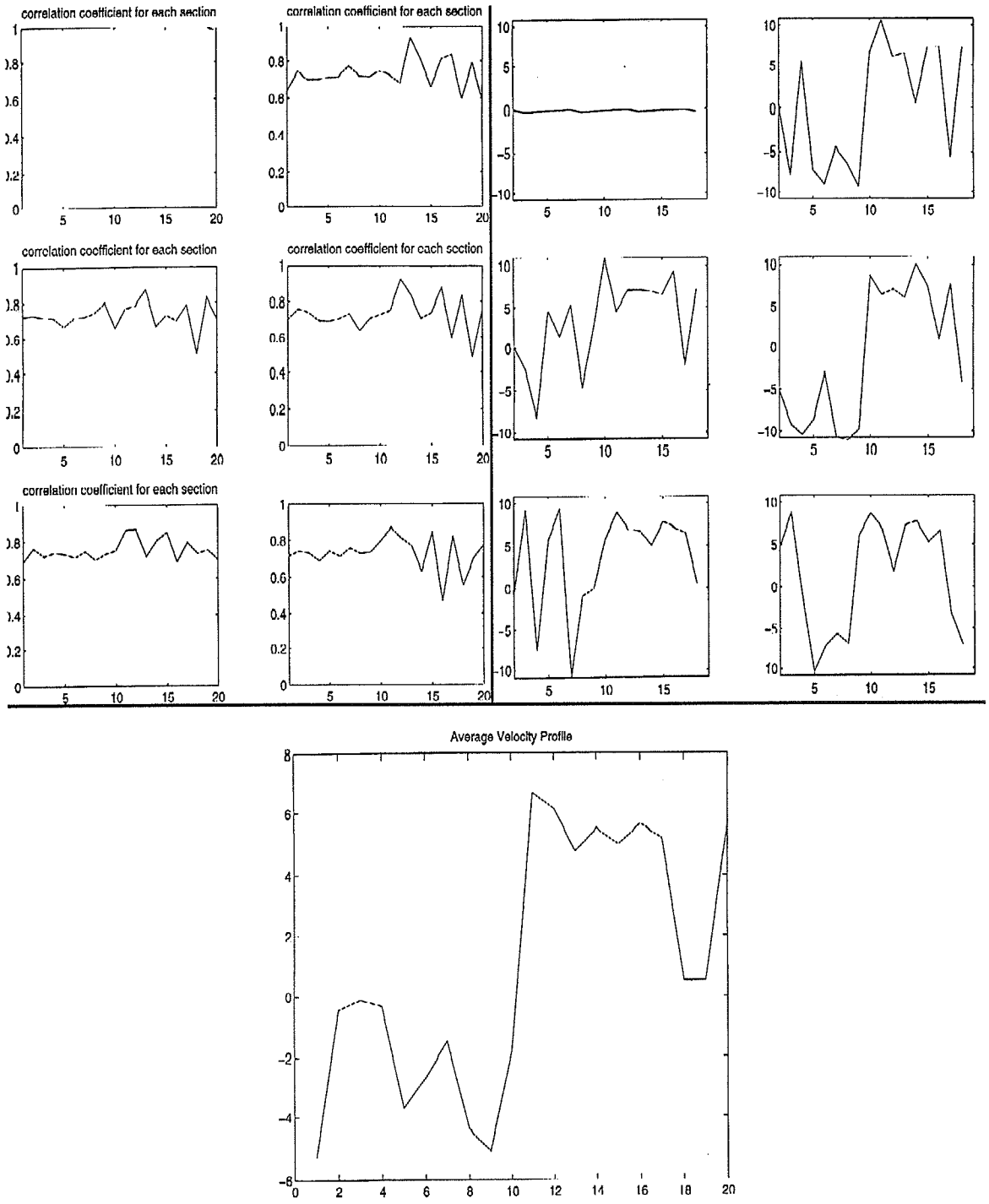


Figure 21. Correlation and displacement results from a motion experiment. Adjacent waves are correlated. The results are generated by dividing the waves into sections.

of Figure 21 represents an average of all the motion profiles in the top right of the figure. The motion is roughly indicated to be occurring in the right side of the waves where the signal is. The left side is closer to zero. It is not exactly zero because there are no distinct features on the left side of the waves for the program to make a good correlation. Consequently the program ends up matching the sections on the left side in a random manner.

As has been demonstrated by this chapter, the correlation technique is able to detect motion and direction. If the motion is continuous, velocity curves can be generated which is the topic of the next chapter.

# CHAPTER 4

# MEASURING FLUID FLOW WITH UTDC

The correlation technique is capable of measuring blood flow in blood vessels. In order to test the technique, a fluid flow was established in a Tygon tube and data collected and analyzed to generate the velocity profiles. The fluid flow phantom , the data acquisition procedure , and the results are presented in this chapter.

## 4.1 Fluid Flow Phantom

To replicate blood flow in a blood vessel, a Tygon tube was chosen to carry a fluid containing added scatterers representing blood. The phantom has a known rate of fluid flow which can be compared with the generated results. It also has the ability to adjust the measurement angle. The fluid flow has to be laminar in order to eliminate turbulence which can invalidate the correlation technique. The condition to develop laminar flow is dictated by [5]

$$Q = \frac{D^4 g \rho_\circ H}{128 \mu L} \tag{10}$$

where $Q$ is the volumetric flow rate ($m^3/s$), $D^4$ is the tube diameter (m), $g$ is the acceleration due to gravity (9.8 $m/s^2$), $\rho_\circ$ is the fluid density ($kg/m^3$), $H$ is the head loss (m) (difference between the source and drain reservoir levels), $\mu$ is the viscosity of fluid ($Ns/m^2$), and $L$ is the total length of the tube (m). For water $\mu$ is 0.001 $Ns/m^2$. Using this equation, appropriate lengths of the tube can be found for a given flow rate and head distance to establish laminar flow. This was done in the phantom to avoid turbulent flow which can distort the sample volume as it moves within the ultrasound beam leading to decorrelation of two adjacent waves. This leads to incorrect correlation results because the best correlation match occurs in the wrong place.

The blood flow phantom is shown in Figure 22. The upper reservoir contains the fluid with scatterers and has one end of a 4 mm diameter Tygon tubing in it. The tubing extends from the upper reservoir to a point which is high enough (as determined from Equation 10) to establish laminar flow. From there it travels in a vertical fashion to reach a water tank where the ultrasound transducer is mounted to collect the data from the submerged tube. The transducer points towards the tube and can be moved spatially in three dimensions to place the focal zone of the transducer within the volume of the tube. This optimizes the returned signal since the energy of the beam is concentrated most at the focal zone. The focal zone and beamwidths for the 15 MHz and 20 MHz transducers have been measured by Kay Raum from the Bioacoustics Research Laboratory and the focal zones are 1.8 mm and 2.15 mm, respectively, and the -6 dB beam widths are 187 μm and 173 μm, respectively.

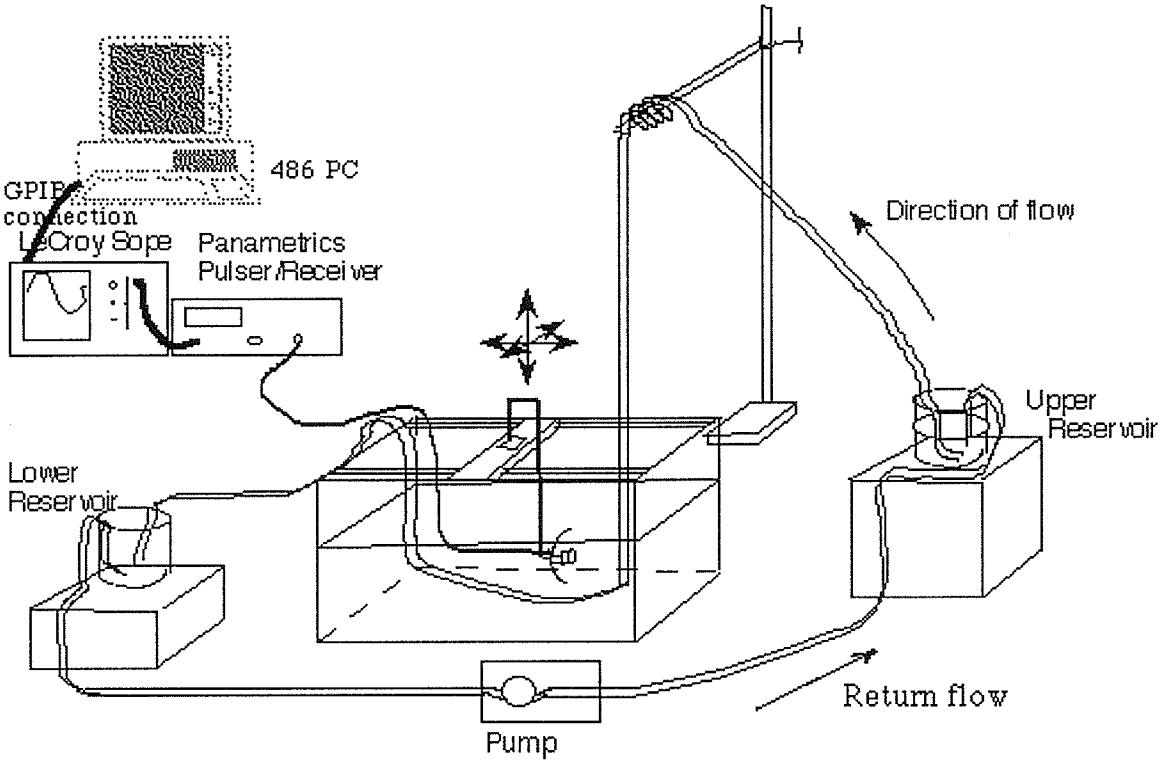


Figure 22. Fluid flow phantom and data acquisition system.

The flow is started by applying suction at the lower end, and once the flow is started, the lower end of the tube is kept below the upper end (siphoning). Once flow is established, the transducer is positioned such that the focal zone is placed approximately in the middle of the tube where the flow is occurring. The transducer is held in place with a device that can rotate it within a 90 degree range. There is also the capability to manually move the transducer in three dimensions to place it in the appropriate place. The angle is chosen to maximize the returned signal. There is a tradeoff between obtaining the strongest signal and obtaining a small angle, which maximizes the amount of time the scatterers stay within the beam. If the angle is too small, the signal is reflected in a direction away from the transducer thereby producing no echo. The maximum angle obtainable with a capturable echo was approximately 45 degrees.

## 4.2 Tubing Material

The material of which the tube is made also affects the signal. Three materials were tried: Tygon plastic, rubber, and dialysis membrane tubing. The Tygon is better at producing a reflection than the rubber and allows a smaller angle for an echo to be measured. The rubber attenuates the signal more and consequently does not produce as strong an echo. Therefore Tygon is preferred to the rubber tubing for the flow measurements. The dialysis tubing produces the best results in terms of both a stronger signal and the ability to minimize the measurement angle. The dialysis tubing has the tendency to expand in diameter after repeated use. After only an hour in water the diameter can expand to three times its original value of 6 mm. It also has an additional benefit of not producing a reflection at the tubing interface. This allows most of the ultrasound energy to be reflected by the scatterers instead of the tubing. Also various diameters were tried for the Tygon and the rubber tubes. The smallest diameter was 4 mm for the Tygon material, which is the tube used to produce the following results. This was chosen so that both sides of the tube could be identified on the returned signal. This is easier to do for a smaller

diameter tube since in a larger diameter tube the signal attenuates to a degree where no echo is produced for the far side of the tube. This compromises the placement of the focal zone in the area of the laminar flow. The smaller tube also captures fewer data points with a greater spatial resolution since the distance which the ultrasound beam has to cover is small. The signal is obtained by visualizing both ends of the tube on the oscilloscope screen. This can be confirmed by having a stationary signal at both ends representing the edges of the tube. The middle represents the fluid portion and with flow the signal from the middle can be seen to produce wave shifts. The wave shifts can be tracked with the naked eye if the slow is extremely slow; otherwise, the signal appears to be noise with faster flow rates.

## 4.3 Scatterer Material

The material for the scatterers was chosen to give the strongest return signal . If there are no scatterers in the fluid, there is no returned echo from the water flow. Some particles have to be mixed in the water to produce an echo. The material has to be suspendable in water so that the particles can distribute evenly and float in the tube. Several materials were tried to determine which gave the strongest signal. From previous work done [1] , Sephadex (G-50; 80-100 μm diameter, Pharmacia Fine Chemicals, Uppsala, Sweden) was tried as a scatterer. It gave a strong and clear signal when compared to the other scatterers but due to its expense and limited quantities available, its use was abandoned in favor of cheaper materials. The next material to be examined was Miracle Gro® plant food. This material partially dissolves in water and also retains solid particles in the solution which are small enough to be carried with the flow in the 4 mm diameter tube. These particles are large enough to be seen with the naked eye whereas the Sephadex particles can not be detected. The signal from Miracle Gro® was also strong but weaker and noisier than Sephadex's signal. It was more difficult to maintain a flow where the Miracle Gro® particles remain in solution since they are large particles which have a

tendency to settle out. Miracle Gro® was able to give a signal from which velocity could be determined. A better material tried later was ordinary talcum powder. This material did not easily dissolve in the water unless it was continuously stirred. The concentration was increased until a strong enough signal was received. The particles once suspended in water stayed in the solution longer than Miracle Gro® and were visible to the naked eye. The talcum powder produced a stronger signal and is easier to handle. This was chosen as the material for measuring flow.

## 4.4 Data Acquisition System

The data acquisition is depicted in Figure 22. The ultrasound transducer is driven by a Panametrics 5800 Pulser Receiver with a bandwidth of 35 MHz. The pulse repetition frequency can be selected in increasing increments up to 10 kHz. The pulser receiver also has an adjustable gain for the transmitted signal. The output from the pulser receiver goes to a LeCroy 9354 TM digital oscilloscope. This scope can sample at a 2 GHz rate with one channel and has a flash memory storage space of 1 Mbyte per channel. This allows extremely fast capture and storage of data. The scope is triggered by the pulser/receiver and can capture a preset number of waves. This feature allows for acquiring multiple waves at one location at the PRF determined by the pulser receiver.

The waves are captured in binary format. The data are then transferred from the scope memory to 486 PC which is connected to the scope by a GPIB connection. A utility in Basic that came with the scope (Wavetran) can convert the binary data into ASCII format on the PC, or alternatively, the binary data can be converted by Matlab. Once the data are on the PC, they can be transferred to a workstation for analysis.

The scope has to be able to capture a wave as well as store it in its own memory or be able to transfer it to another storage device as fast as the PRF set on the pulser receiver. If the data capture is slower, the particles can move out of the beam before the next wave is captured. This was a major stumbling block in this work since the fast LeCroy scope was

not available in the beginning of the work. The previous scope, Tektronix 11401, could sample fast enough but lacked the ability to store the data fast enough or the ability to transfer it fast enough to the PC hard drive over a GPIB connection. This rate limiting transfer rate resulted not from the GPIB connection but from the software written to communicate with the Tektronix scope. Even after optimization of the communication software, the fastest transfer rate achieved was 40 ms between two waves. This time is too long for measuring flow rates where the particles do not settle out of solution. Therefore a decision was made to purchase the LeCroy scope.

## 4.5 Relationships Determining Flow Rates

The volumetric flow rate, the diameter of the tube, the PRF, the beam width, and the measurement angle all interact to determine the linear flow rates which can be measured and each variable places limitations on the other. In this section the relationships among the various parameters will be explored.

There are two definitions of flow rate used in this thesis, volumetric flow ($cm^3/s$) and linear flow (cm/s). In order to measure the volumetric flow, flow rate is determined by measuring the amount of water that is collected in a graduated cylinder in a given amount of time. This volumetric flow rate is converted to a linear flow rate by dividing the volumetric flow rate by the cross-sectional area of the tube. The linear flow rates are plotted as the velocity profiles. For a given volumetric flow rate, a smaller diameter tube provides a faster linear flow rate and a larger diameter tube provides a slower linear flow rate.

One of the parameters that can not be adjusted is the beam width. If it is assumed to be 150 μm, which approximately is the correct value for the 15 and the 20 MHz transducers, and the angle is assumed to be 90°, which is the worst angle that can be used since the axial component of flow (in the direction of the beam) is zero, the distance the scatterers can move while remaining within the beam is 150 μm, same as the beam width. If the angle is decreased to 45°, the scatterers get a larger area, $\sqrt{2}$ times more distance

(212 μm) to be insonated by the beam. If the angle is decreased further to 20°, the distance increases to 2.9 times the original (435 μm). As the angle decreases further, the distance increases rapidly (for 10° the distance is 5.8 times the original). To increase the time scatterers spend within the beam, we can decrease the angle, but beyond 45° the echo is lost due to reflection.

Choosing a lower angle relaxes the requirements on the PRF for a given flow rate. At a given flow rate and an angle which optimizes the distance for the scatterers to be insonated (small angles), the waves can be captured at a slower rate (PRF) because the scatterers stay within the beam for a longer period of time. This occurs because the effective beam width becomes wider and for the given flow rate , more time can be allowed for the scatterers to move out of the beam.

Similarly, choosing a slow flow rate for a given angle relaxes the requirements on the PRF. The slower the scatterers move the more time there is to capture the two adjacent echoes before they move out of the beam. Conversely the requirements on having a small angle and slow flow rate can be relaxed if the PRF is increased.

For an effective beam width of 212 μm (45° angle), PRF of 1 kHz(T=1000 μs), and a tube diameter of 4 mm, linear flow rates of up to 20 cm/s and volumetric flow rates of 2.51 $cm^3/s$ can be measured. With the fastest PRF available(10 kHz), measurable linear flow rates increase to 200 cm/s and volumetric flow rates increase to 25.12 $cm^3/s$.

## 4.6 Results

Several flow and measurement conditions were explored to see how the algorithm performed. In the following results talcum powder was used as a scatterer and a 4 mm diameter Tygon tube was used to carry the water and talcum powder mixture. A 10 MHz Panametrics focused ultrasound transducer was used instead of the 15 or the 20 MHz transducers available because it produces a wider beam and its beam is able to penetrate the

tube for a longer distance. The actual beam width has not been measured but a theoretical beam width was calculated and used to determine flow conditions according to

$$beamwidth = \frac{1.44\lambda ROC}{D} \tag{11}$$

where $\lambda$ is the wavelength ($\lambda = c/f$, $c$=1520 m/s, $f$=10 MHz), $ROC$ is the radius of curvature (51 mm), and $D$ is the diameter (25.5 mm). The beamwidth is calculated to be approximately 438 μm.

Figure 23 displays the average velocity profile from a typical flow experiment. This graph was generated after averaging 23 individual velocity profiles. The y axis represents

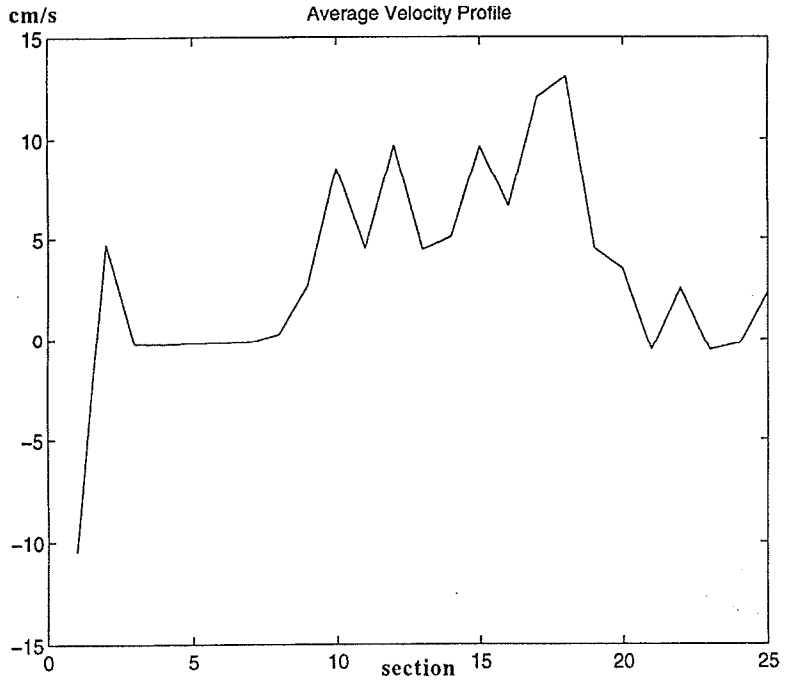


Figure 23. A typical averaged velocity profile generated from 23 individual waves.

flow in cm/s and the x axis represents the cross section of the tube divided into 25 sections. The experimental conditions were linear flow rate-5.4 cm/s, PRF-1 kHz, and measurement angle-50°. Although it is not smooth, a rough flow profile can be seen in the middle of the graph. Both ends of the graph are at zero except for the end points because of the inability to correlate the end sections in both directions as explained previously. In Figure 24 several

representative echoes, individual flow velocity profiles, and the corresponding correlation curves from this data set are shown.

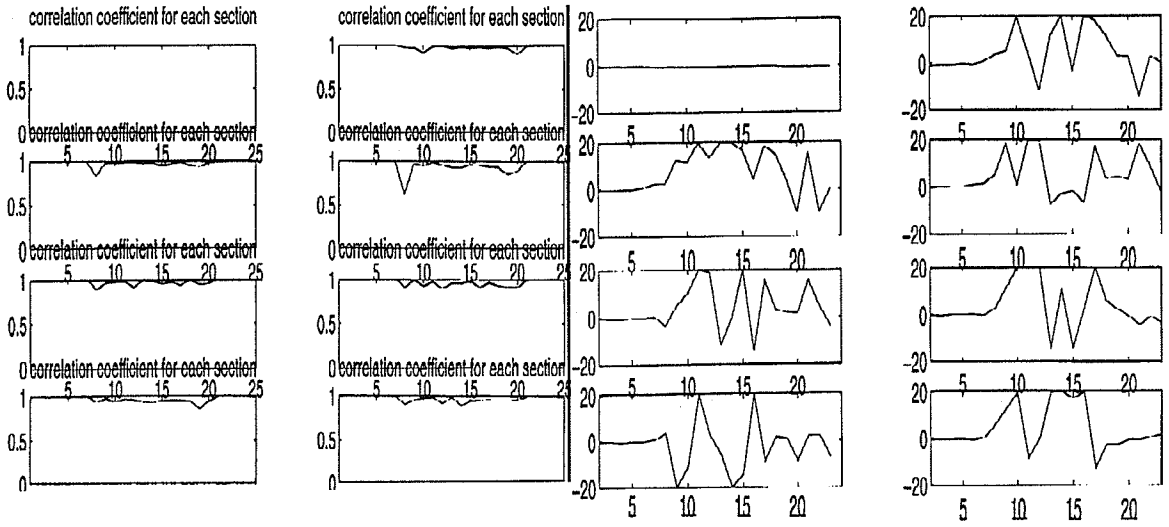


Figure 24. Typical individual correlation curves and velocity profiles used to generate the averaged velocity profile.

Figure 25 shows an average velocity profile made from 23 individual velocity profiles of another data set. The experimental conditions were linear flow rate-19.2 cm/s, PRF-1 kHz, and measurement angle-50°. This graph clearly shows a parabolic velocity profile at 18-19 cm/s. The same decorrelation effects are seen at both ends.

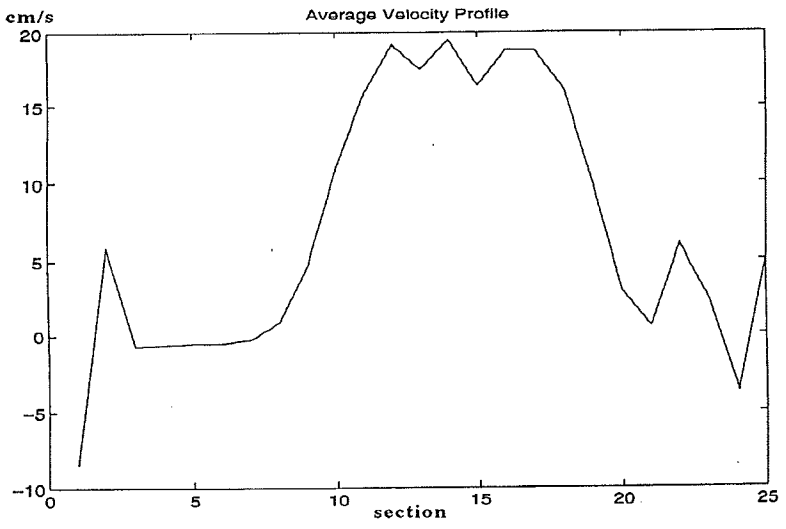


Figure 25. Average velocity profile. Flow rate was 19.2 cm/s. PRF was 1 kHz.

Figure 26 shows a similar curve where the same flow conditions applied but the PRF was raised from 1 kHz to 2 kHz. The curve is more uniform at the top indicating a more consistent shift in the correlations. This occurs because the data are collected twice as fast and there is less chance of decorrelation since the shift is smaller and more consistent. The wave has less chance to decorrelate and keeps its shape better from pulse to pulse.

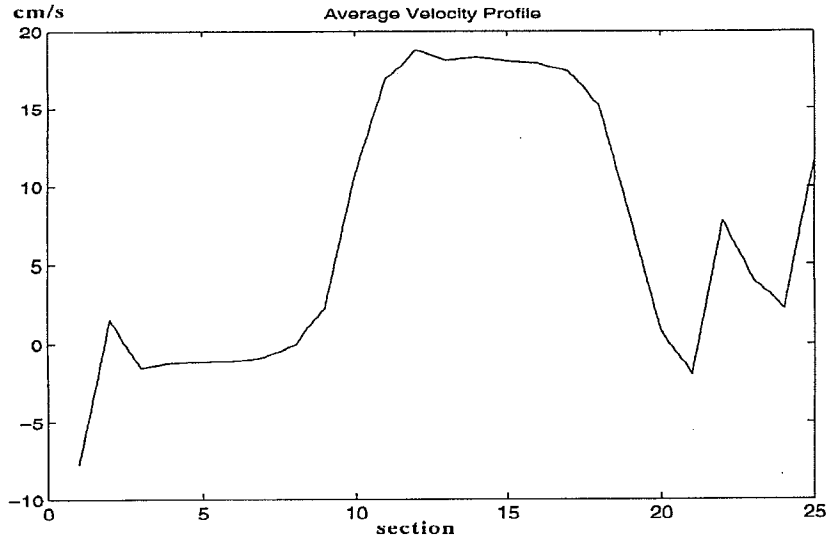


Figure 26. Averaged velocity profile. Flow rate was 19.2 cm/s. PRF doubled to 2 kHz.

In another experiment the flow measurement conditions were changed to give an increased angle of 80° from 50° decreasing the axial component of flow (made worse). The PRF was raised to 10 kHz from 2 kHz, the maximum available. The linear flow was maintained at 19 cm/s. The average of four individual velocity profiles is shown in Figure 27. This is much less smoother because only four individual velocity profiles are averaged. The peak flow rates shown in the graph reach values of 60 cm/s. This can be attributed to a large measurement angle which is closer to 90°. At angles that are closer to 90°, it becomes harder to measure the actual angle and the calculated velocity can vary greatly as the angle approaches a right angle. These two effects can give results that do not match the measured flows.

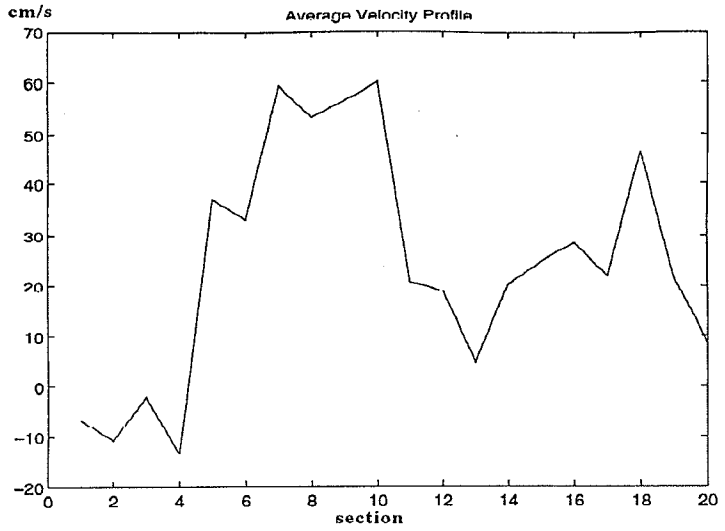


Figure 27. Averaged velocity profile from four individual waves. Angle made larger (worse) from 50° to 80° and the PRF raised fivefold to 10 kHz.

Figure 28 shows the results from the same data except 15 waves are averaged. The velocity profile is smoother but not as smooth as Figure 26 where the measurement angle was 50° and 23 waves were averaged. The rougher curve in Figure 28, when compared to Figure 26, could be explained either as being averaged from a fewer number of waves (15 vs. 23) or having a larger measurement angle (80° vs. 50°). Even though the PRF in Figure 28 is 5 times higher, it is not enough to compensate for a larger measurement angle.

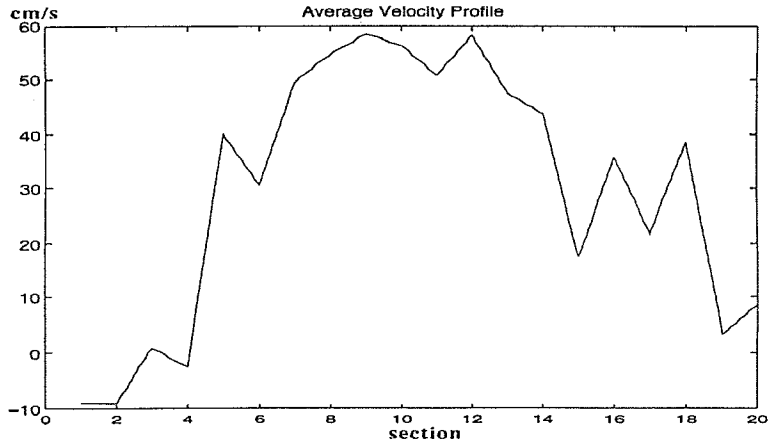


Figure 28. Averaged velocity profile. PRF=10 kHz, averaged from 15 waves, measurement angle=80°.

In Figure 29 the same flow rate of 19 cm/s and measurement angle of 80° were

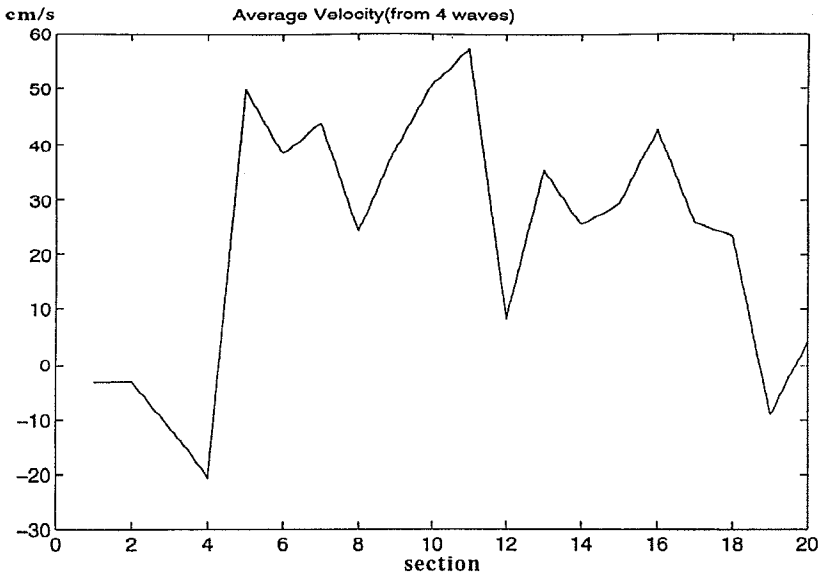


Figure 29. Averaged velocity profile. PRF halved to 5 kHz, averaged from 4 waves, measurement angle=80°.

maintained but the PRF was reduced from 10 kHz to 5 kHz. The flow rate is still biased towards higher values by the larger angle as before. This average velocity profile is made from four individual velocity profiles. The resulting velocity profile is much less smooth. This can be due to two reasons. The first one is that only four waves are averaged instead of 15 as in Figure 27. The second is that the PRF is halved to 5 kHz. It is difficult to separate the two but the individual correlation profiles from each experiment can be compared to see if the correlation curves from the faster PRF experiment showed higher correlation values. The correlation curves from the 4 wave and the 15 wave experiments are shown in Figure 30. The graphs in Figure 30 do not, in general, show higher correlation coefficients for the case in which the PRF is higher (10 kHz). Therefore the explanation that when the PRF is halved, the correlation values decline for this flow rate is inaccurate. With the given flow rate of 19.2 cm/s and a PRF of 5 kHz, the scatterers travel a distance of 390 μm between two pulses. This distance is less than the effective beam width of

441μm at this angle. Therefore the 5 kHz PRF is just fast enough to track the scatterers before they move out of the beam. This is why there is no significant difference in the correlation values.

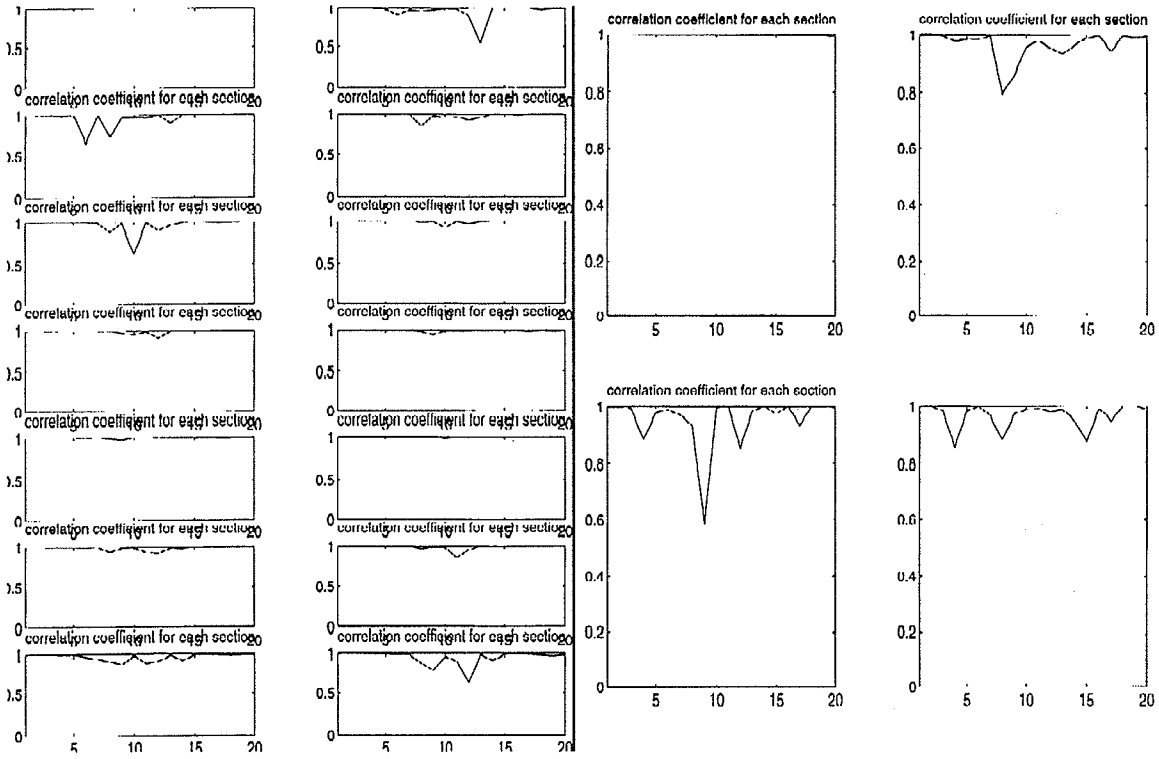


Figure 30. Correlation curves from the 15 wave (10 kHz) and 4 wave (5 kHz) experiments.

In Figure 31 the flow rate is doubled to 38 cm/s while the PRF is kept at 5 kHz with the same angle (50°). The graph is completely decorrelated because the scatterers are moving twice as fast. They do not stay within the beam for the 200 μs allowed by the 5 kHz PRF for two adjacent waves to be tracked. As calculated above the distance the scatterers moved at 19.2 cm/s was already near the beamwidth of the transducer. Any increase in flow rate or decrease in PRF at those conditions would be expected to produce decorrelated results as in Figure 31.

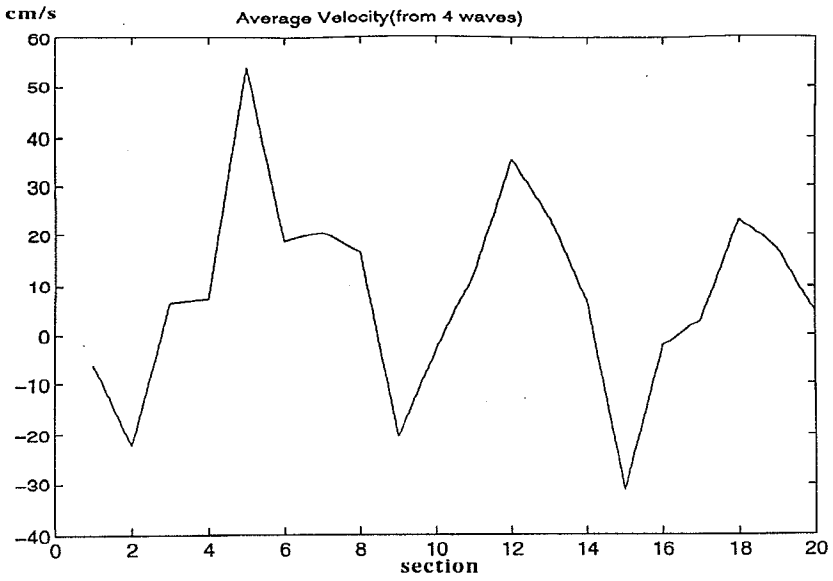


Figure 31. Averaged velocity profile. PRF=5 kHz, averaged from four waves, measurement angle=80°. Flow rate being doubled results in complete decorrelation.

Increasing the PRF would be expected to restore the velocity profile to a somewhat parabolic shape. In Figure 32, the PRF is increased to 10 kHz from 5 kHz. A velocity profile similar to Figure 29 is restored. The two times faster PRF is able to track the scatterers twice as fast with roughly the same degree of accuracy.

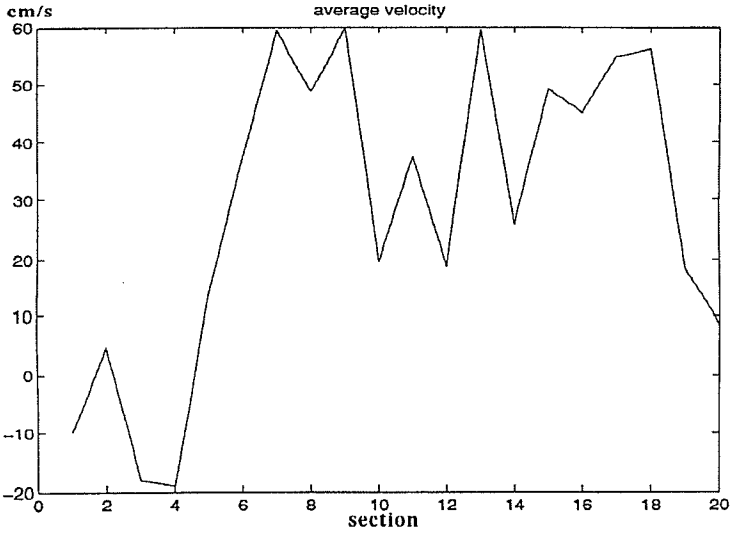


Figure 32. Averaged velocity profile. PRF=10 kHz, averaged from four waves, measurement angle=80°. PRF being doubled results again in targets being tracked.

The following set of results demonstrate the effect of limiting the correlation search area. Flow was established in the Tygon tube but it was reversed in direction. The linear velocity was 19.2 cm/s and the angle was approximately 80°. At this angle a difference in even one or two degrees can cause large shifts in the value of the flow rate. This did occur in the results and therefore the values for the flow rate are inaccurate and unreliable. Even so, other features in the graph are worth noting. Figure 33 shows two velocity profiles,

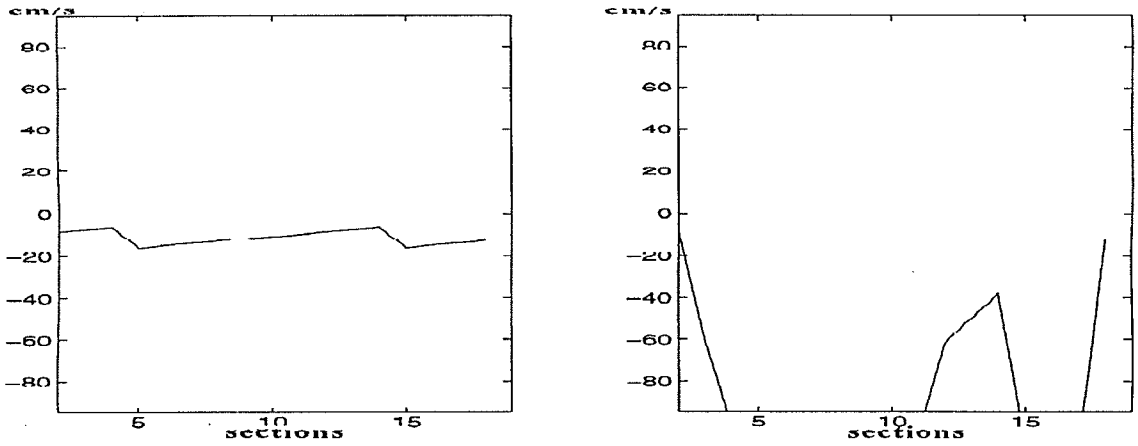


Figure 33. Two individual velocity profiles. Amount of shift for search area is 10 pixels in both directions.

the left one due to correlating the first wave with itself and the right one due to correlation of the first wave and the second wave. The first feature to be noticed is the reversal in direction of the flow. This demonstrates the ability of UTDC to determine direction without additional calculations. In this figure the searchmaxvel input parameter was not used but the search area was limited to 10 pixels on both sides of the original sections. The graph shown on the right of Figure 33 is the result. The velocity profile has reached a maximum value ( negative in this case because of reversed flow) and stays there for most of the sections. From this it can be said that the limit placed on the search area, 10 pixels, is too small because all the sections consistently matched at the same distance giving a flat profile. This distance turns out to be 10 pixels after plugging in the known values in the velocity formula. The scale on the y-axis is in centimeters per second but in this case a shift of 1 pixel also equals 10 cm/s on the y-axis. The graph could not search beyond the ten pixels

and consistently matched at this limit. This indicates that the actual shift must be greater than the 10 pixels.

To explore this point further another set of graphs was generated from the same data set which is shown in Figure 34. Four graphs are shown instead of two. This time the shift was increased to 20 pixels on both sides. The graphs take on a more parabolic shape as expected in laminar flow. The magnitude also increases from -95 to -200 indicating that doubling the search area also doubled the flow rate. If increasing the search area further does not produce a change in the shape of the profiles , it can be assumed that the maximum shift has been found and increasing the search area further is not going to produce better results. In contrast, increasing the search area can produce worse results because there is more likelihood of matching the original sections with the wrong new sections. The search area was increased to 40 pixels on both sides and the results are shown in Figure 35. The profiles retain their shape with the exception of a few points.

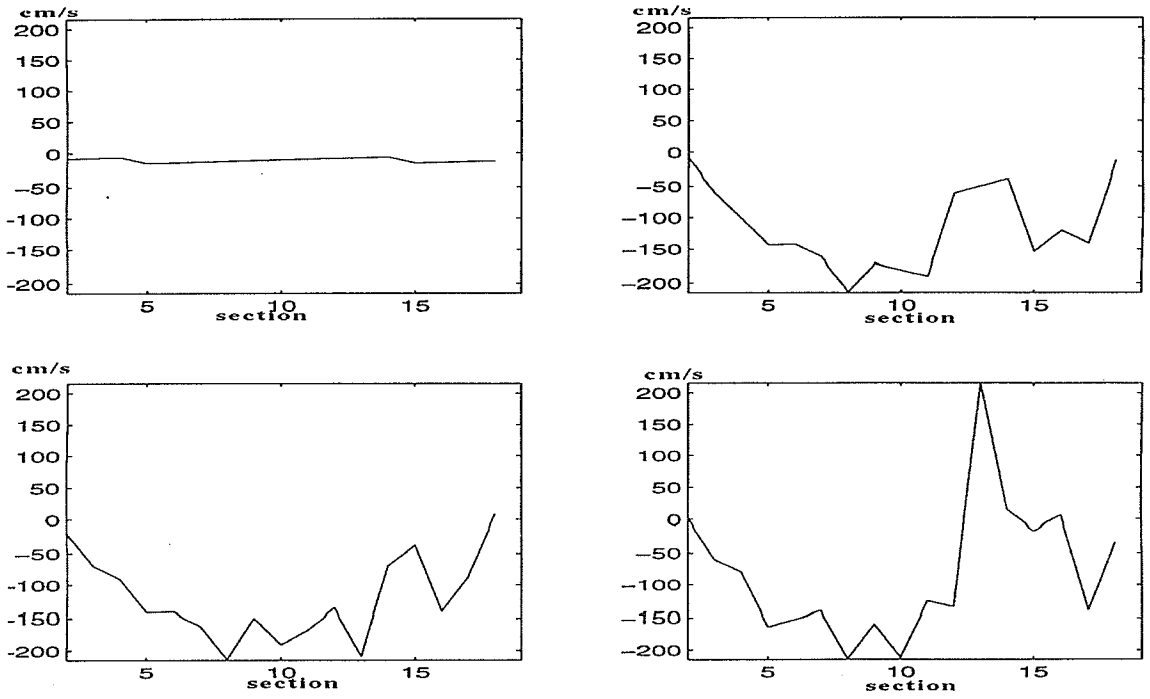


Figure 34. Velocity profiles generated by searching 20 pixels in both directions.

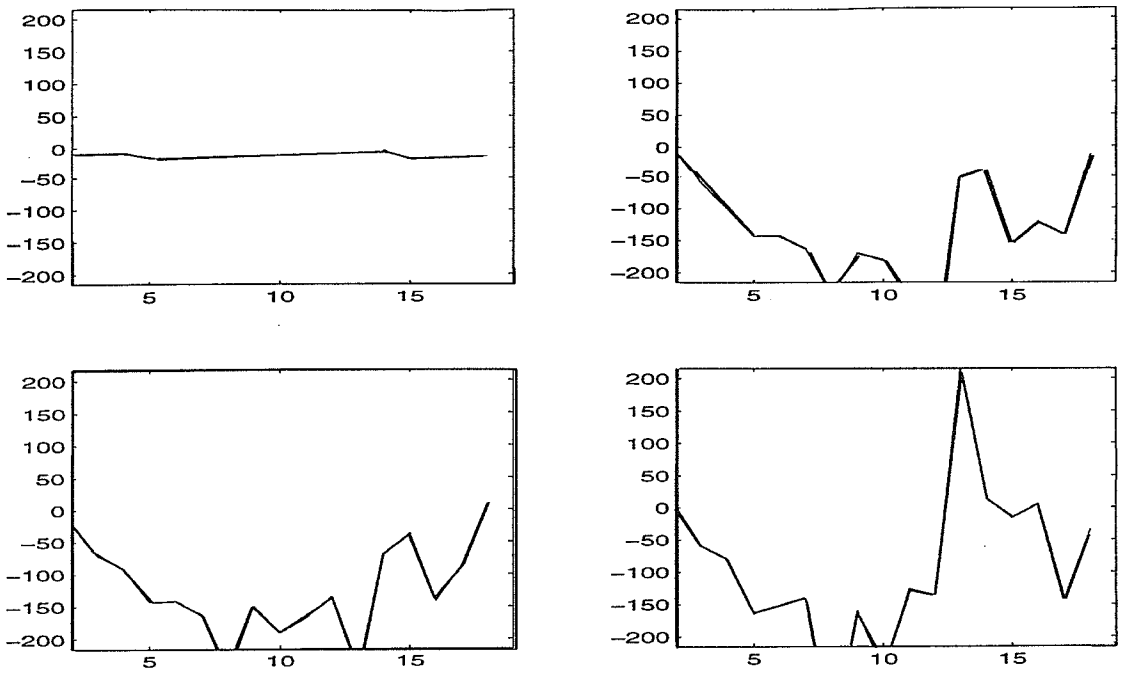


Figure 35. Velocity profiles generated by searching 40 pixels in both directions.

The results have shown clearly the ability of UTDC to measure flow rates and determine direction of flow. The next chapter tests the UTDC technique in a live animal.

# CHAPTER 5

# BLOOD FLOW MEASUREMENTS IN THE GUINEA PIG

The UTDC technique has been demonstrated in a flow phantom. It can measure flow under controlled conditions such as large diameter tubes. An extension of the technique is now presented where it is applied in the live guinea pig to see if it is capable of measuring real blood flow. The measurements were taken in several organs of the guinea pig in vivo. The technique and results are presented in this chapter.

## 5.1 A Realistic Flow Model

The UTDC has been applied in humans and is able to give blood flow velocities with large vessels. It has to be tested under real blood flow conditions in this work such as a guinea pig to see how it performs. With a live animal model, this is possible. The live guinea pig provides the opportunity to measure flow in various organs, each with a different anatomy and flow conditions. The flow conditions in a real physiological model are complex and unpredictable. The complexity of the measurement conditions is what is explored in this chapter.

### 5.1.1 Physiological kidney phantom

Prior to attempting the measurements in the guinea pig model, another model was explored for measurement of flow. Although not in a live animal this is a physiological model. This model is capable of providing actual physiological flow conditions. However, it was not utilized due to some of the difficulties to be mentioned shortly. Developed by Dr. Ken Holmes of the Veterinary Science Department at the University of Illinois, the model is an actual pig kidney excised from a pig and treated with several alcohol washes to preserve the architecture of the kidney's vasculature. The kidney is capable of being stored in the

alcohol solution for years and has the ability to be reused at a later time. After the kidney is preserved in a concentrated solution of alcohol, it can be used again to establish flow after going through several washes of decreasing concentrations of alcohol until a final wash with water. The different solutions are pumped into the kidney via the renal artery and collected via the renal vein. The perfusate travels just like blood through the vasculature including the capillary network. The kidney model has been used previously for ultrasound heating experiments. The perfusate in those experiments was a solution without any particles. The experiments to measure flow require some particles in the solution that can mimic the red blood cells and reflect ultrasound to produce echoes. There is an additional requirement in the kidney phantom that the particles be smaller than the capillary diameters of 7-10 μm. If they are larger they can plug the capillary network and make the kidney useless for flow measurements.

### 5.1.2 Scatterer materials for the kidney phantom

Two things were explored as scatterer materials, Albunex and Zeospheres®( 3M Company, Minneapolis, MN). Albunex is a solution of bovine protein bubbles in water created by using a low frequency ultrasound horn to mix the two in a solution. The albumin protein forms round hollow air-filled spheres with average diameters of 3-5 μm. This material is also used as a clinical contrast agent in ultrasound imaging. For imaging kidney flow the small diameters of the bubbles are desirable. A small quantity (5 mL) of the Albunex was made at the Sonochemistry Laboratory in the Department of Chemistry. It was, however, not utilized because the decision was made to conduct flow experiments directly in the live animal model. Similarly, the second material to be examined was Zeospheres®, a powder material consisting of ceramic spheres with diameters of 2-3 μm. This material is used in making specialty paints or plastic materials. It was examined for its

reflective properties and found to be not as good as the talcum powder. It did have a reflective component that could be measured. However, under the microscope, the small spheres tended to clump together and form larger balls. This consideration and the lack of enough Albunex shifted the emphasis towards real animal experiments.

## 5.2 Guinea Pig Measurements

### 5.2.1 Guinea pig surgery

Adult guinea pigs were used to take flow measurements with the 15 and the 20 MHz transducers of several organs including the kidney, stomach, liver, and inferior vena cava. The animals were first anesthetized with a mixture of Ketamine and Xylazine with an intramuscular injection (0.1 mL per 100g body weight of a solution containing 87 mg ketamine/13 mg xylazine per mL). The anesthetics usually took effect in 5 minutes and the animal was pain free after a few more minutes.

An incision was made in the midline of the animal from the pubic symphisis to just below the xyphoid process, being careful not to injure the diaphragm so that the animal could continue to breath on its own. After entering the peritoneal cavity, the intestines were mobilized to the right side of the body exposing the liver. The viscera were also relocated so that the inferior vena cava and the aorta could be exposed just above the spinal column. The kidney was also exposed. The animal was submerged in a warm saline water bath keeping the mouth out of the water so it could breath. The water is necessary as an ultrasound conducting medium. The animal was held in place by tying the arm and legs in place to a wire screen. The transducer was moved into place using the Daedal system.

### 5.2.2 Problems in data acquisition

Several very serious problems arose in the course of measurements. The most serious one was that of getting good exposure. It was extremely difficult to obtain and maintain a good exposure because the viscera tended to move around in the water. They

often occluded the transducer and delayed measurements in the anesthetized animal. The organ to be imaged also did not stay stationary and moved with water currents, in effect, tending to float to the top. The second problem was due to bleeding. When a bleeder was encountered, it immediately would impair the area of interest from being further explored because the blood was not being removed fast enough from the site. In addition the blood in the immediate vicinity of the organ of interest impaired the ultrasound signal and caused so much noise in the echo that it did not contain any useful information. The area had to be cleared of the water containing blood and replaced with fresh saline.

Another major problem was to locate a meaningful signal even after the other problems were solved. The focal zone had to be placed in the area of interest and it was difficult to assess exactly where that point in space was. A device was designed for the 15 MHz transducer that pointed to the focal zone so that the focal zone could be located without having to measure distances in very small places. It actually took up too much space in the area of interest and the viscera tended to occlude the point in space by surrounding the pointer. The return signals were often very weak or very noisy. The situation was made worse by the animal's breathing movements that tended to move the target out of the focal zone.

## 5.3 Data Collection

Several animals were used to make measurements and data were collected with the 20 MHz transducer. This transducer is the smallest available and the focal zone is closest to the surface of the transducer, thereby eliminating some of the problems of having to clear more of the area around the measurement area. The transducer was attached to the Daedal positioning system. Twenty consecutive echoes were collected at a time by the transducer. After collecting twenty echoes, the transducer was moved to another location in a line formed to image the organ. The distance moved (30-50 μm) was less than the beamwidth of the transducer. Data were collected at a hundred such points across the organ, each point

collecting twenty echoes. The data were also collected across the organ so that a B-mode image of the organ could be formed from one of the twenty waves collected across the 100 point line. The idea was to be able to see the structure of the organ and at the same time determine the blood flow profile at a given location. The B-mode images were constructed from individual A-lines by a program provided by Kay Raum and Kate Frazier of the Bioacoustics Laboratory that reduces noise in the A-lines by filtering them with an appropriate bandpass filter, the filter being constructed by looking at the frequency response of the transducer. After filtering, the Hilbert transform was used to obtain an envelope function. Also the signal was compensated for tissue losses at a rate of 0.75 dB/mm.

The blood flow information is contained within the signal that comes from the stationary structures of the organ. The structures that have the least tissue to degrade the signal and have the largest blood flow are the abdominal aorta and the vena cava. The vena cava sits on top of the aorta in the abdominal cavity and is easier to image. This organ would be expected to give the most accurate blood velocity profiles since there is a large volume of blood flow. In the kidney and the liver the microstructure of the tissue is such that the blood can flow simultaneously in many directions. Measuring blood flow in such conditions can be extremely difficult because of the volumes and the microstructure being examined.

## 5.4 Guinea Pig Blood Flow Results

### 5.4.1 B-mode images

In one of the experiments the kidney and the liver were excised after the animal had died and imaged in saline with a scanning motion of the 20 MHz transducer to create a B-mode image. Figure 36 shows an image of a fresh liver just excised from the guinea pig in saline. The x scale is correct in all the images but the y axis does not represent distance

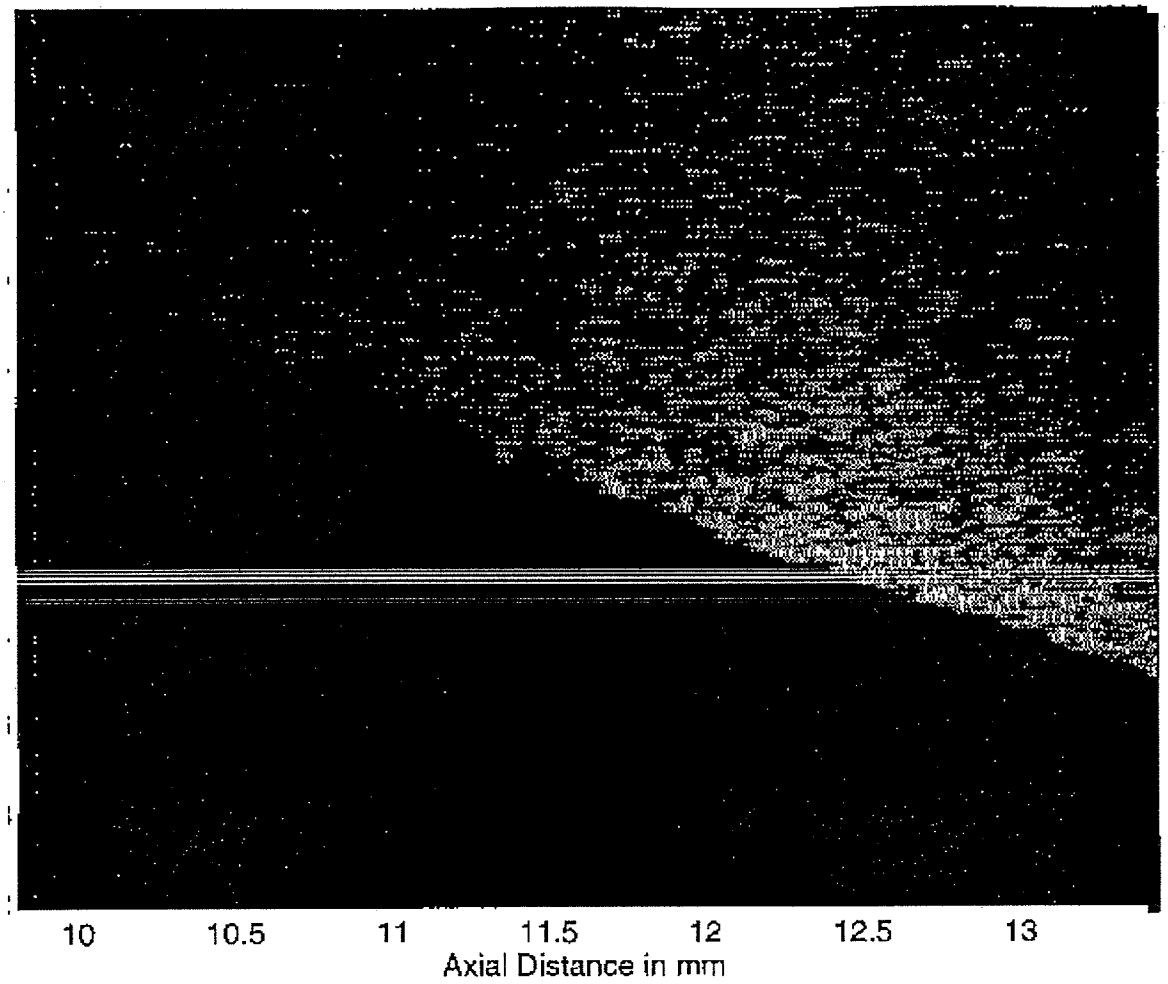


Figure 36. Excised fresh guinea pig liver in saline imaged with a 20 MHz transducer.

accurately. The liver-saline boundary can clearly be seen. The image of the liver has a distinct pattern seen only in the liver image. This uniform pattern is due to the uniform structure of the liver in the area in which it was taken (near the surface).

Figure 37 shows an excised kidney in saline imaged with a 100 MHz transducer. This transducer was available briefly and only one image was taken using this transducer and its pulser/receiver. The image shows the boundary of the kidney on the left side and a distinct feature toward the top of the picture. The resolution of this transducer is much higher and therefore the y-scale is small. The structure seen on top seems to represent a different layer of tissue with the boundary between the top and bottom tissue being more echogenic.

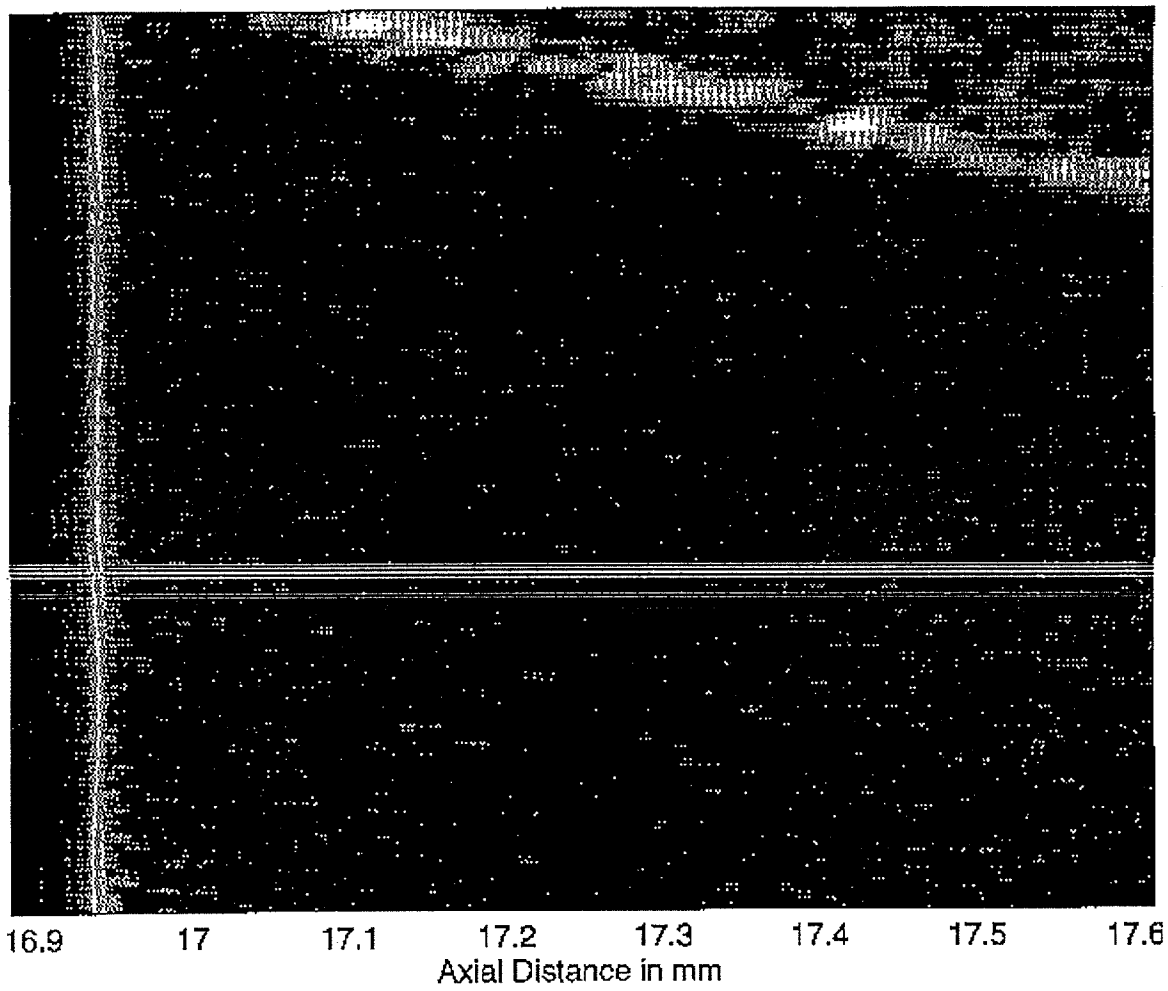


Figure 37. Excised fresh guinea pig kidney in saline imaged with a 100 MHz transducer.

Figure 38 shows an image of a fresh blood clot in saline. There are three layers that can be identified in the B-mode image suggesting that the clot actually has several zones of different acoustical properties. It could be a function of the clotting mechanism, perhaps, representing the activity of fibrin.

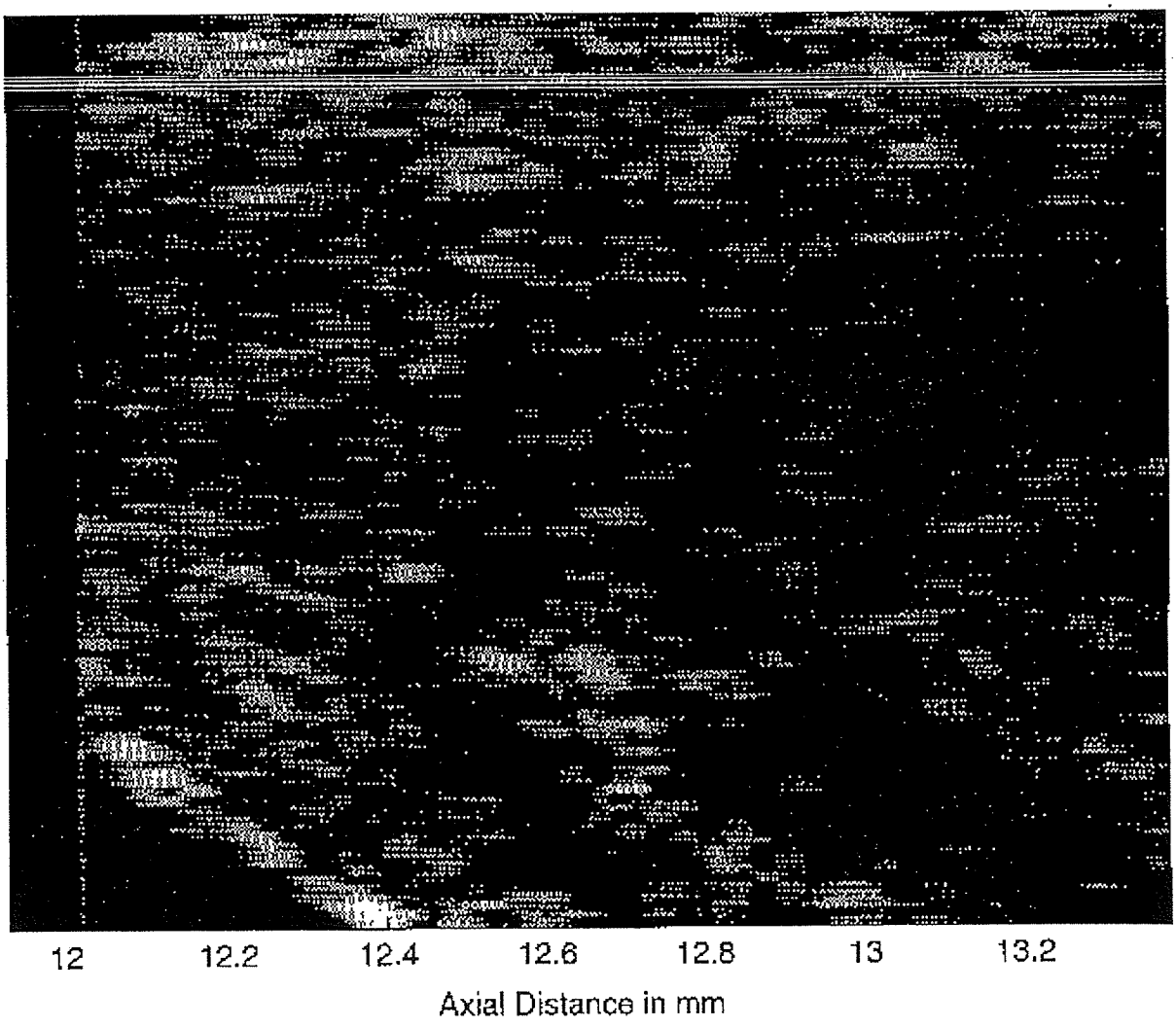


Figure 38. Fresh blood clot in saline imaged with a 20 MHz transducer .

Another set of images were taken in vivo in a live guinea pig of the vena cava, liver, and, stomach.

In Figure 39 the abdominal vena cava is imaged. There is a circular pattern to the image perhaps representing the circular vena cava. It is difficult to identify any distinct features in these images since they are very noisy.

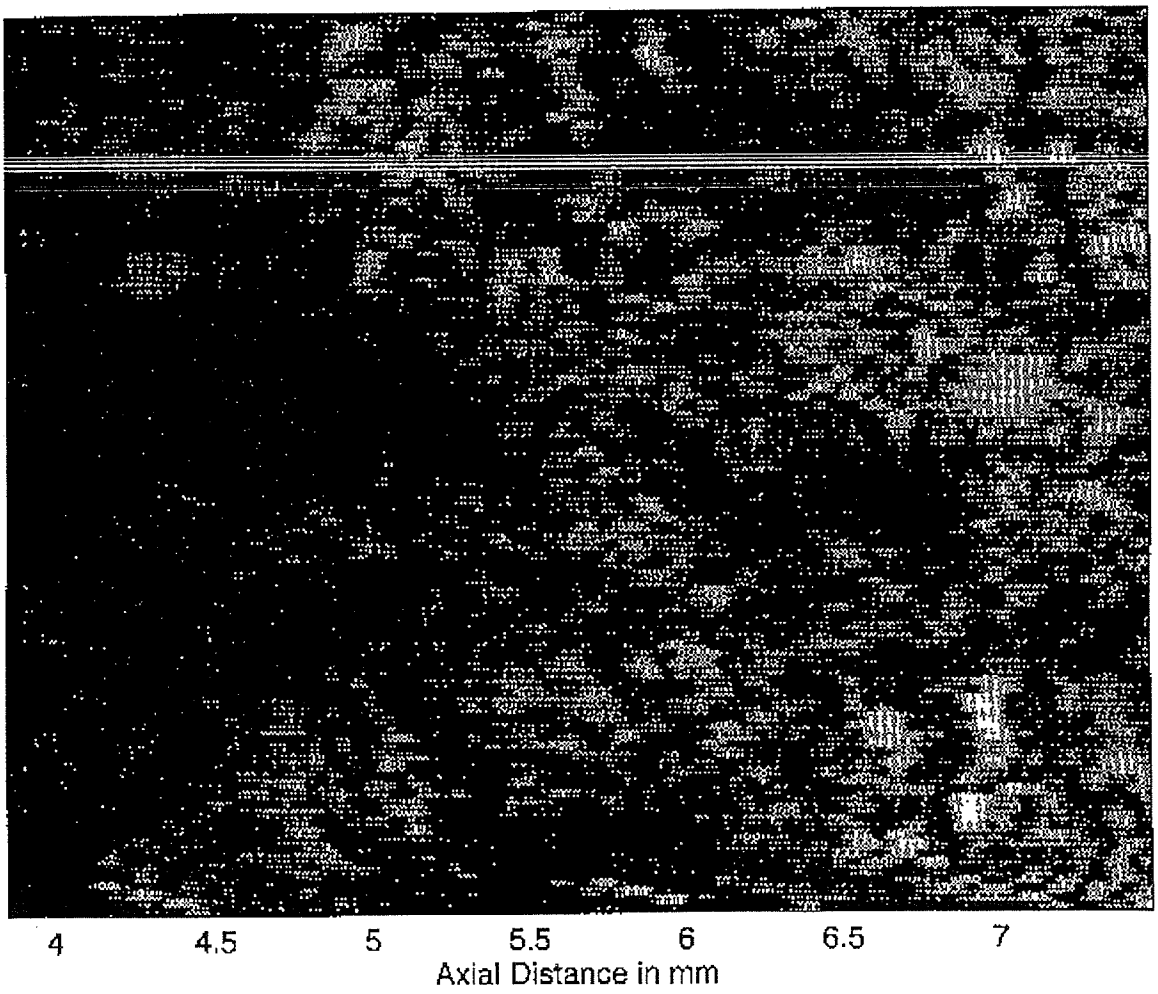


Figure 39. Guinea pig abdominal vena cava imaged in vivo with a 20 MHz transducer.

Figure 40 shows another image of the liver except this is in vivo. A similar liver-saline boundary can be seen. The horizontal white lines are an anomaly that is hard to explain.

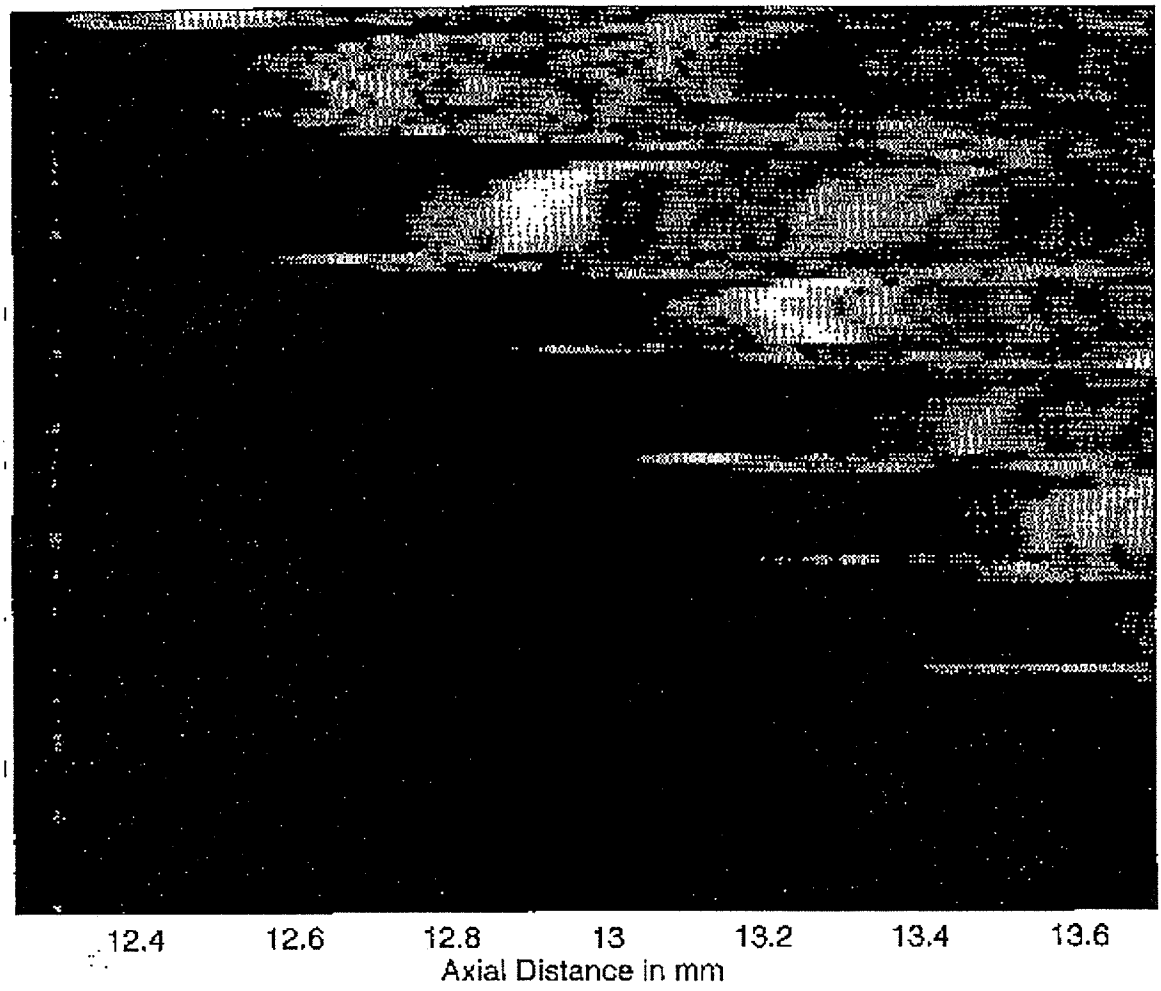


Figure 40. Guinea pig liver imaged in vivo with a 20 MHz transducer.

Figure 41 shows the guinea pig stomach in vivo. The stomach was filled with fluid. The bright area on the left of the image can be explained as the stomach wall and the dimensions of the wall correlate well with the image scale.

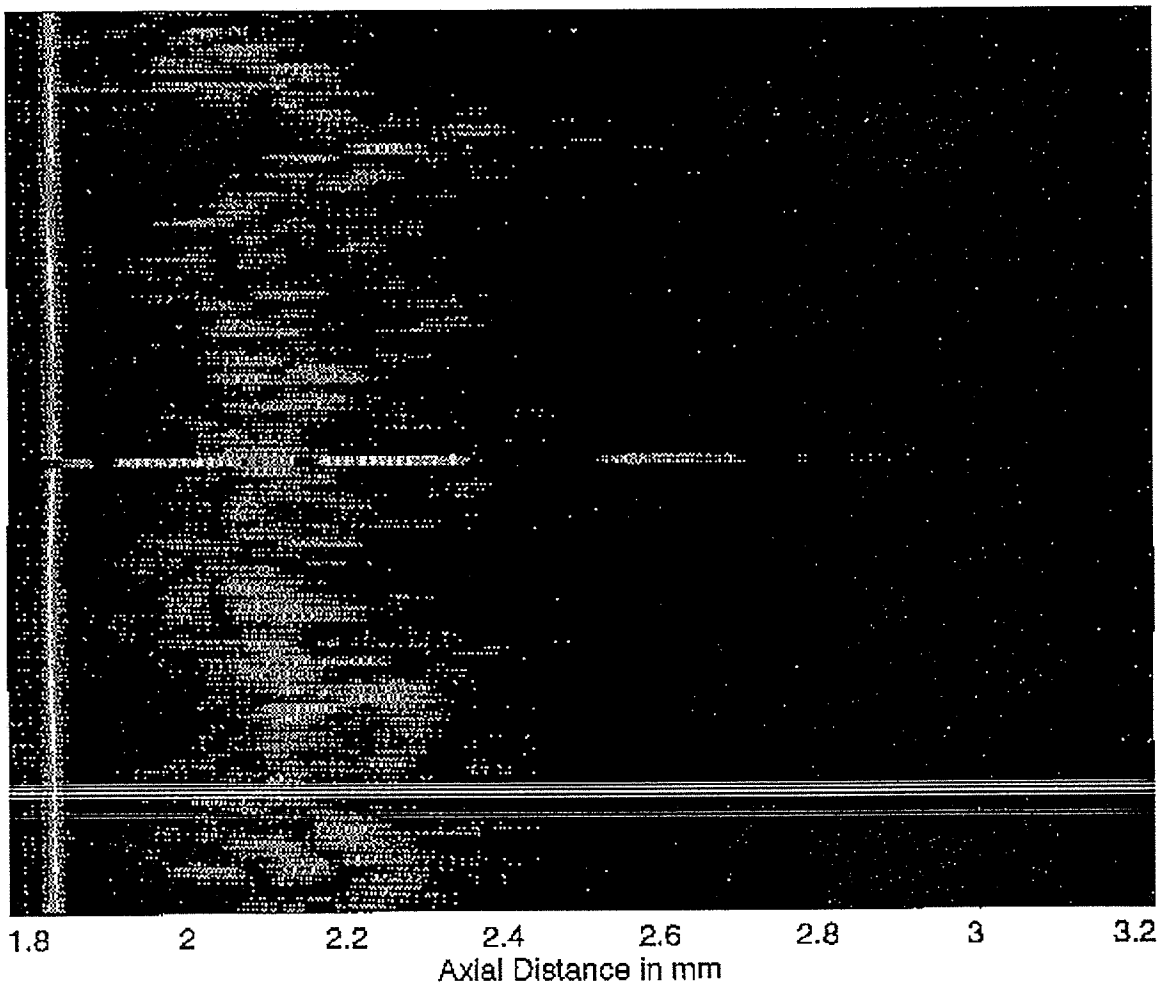


Figure 41. Guinea pig stomach in vivo imaged with a 20 MHz transducer.

5.4.2 Blood flow results from the live guinea pig

A set of four consecutive waves in the in vivo vena cava data set were looked at and analyzed by the correlation program. Each individual wave is 10,000 points long and is shown in Figure 42. The corresponding velocity and correlation profiles are shown in Figure 43. The wave was divided into 200 (50 points long) sections and shifted right and

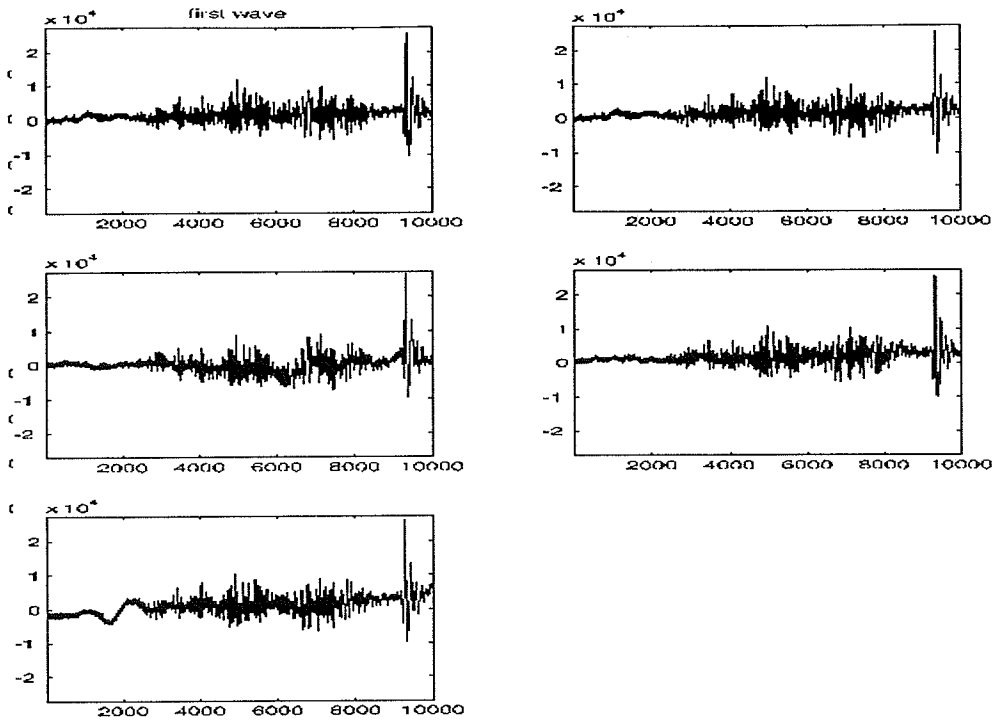


Figure 42. Guinea pig blood flow data-vena cava waves.

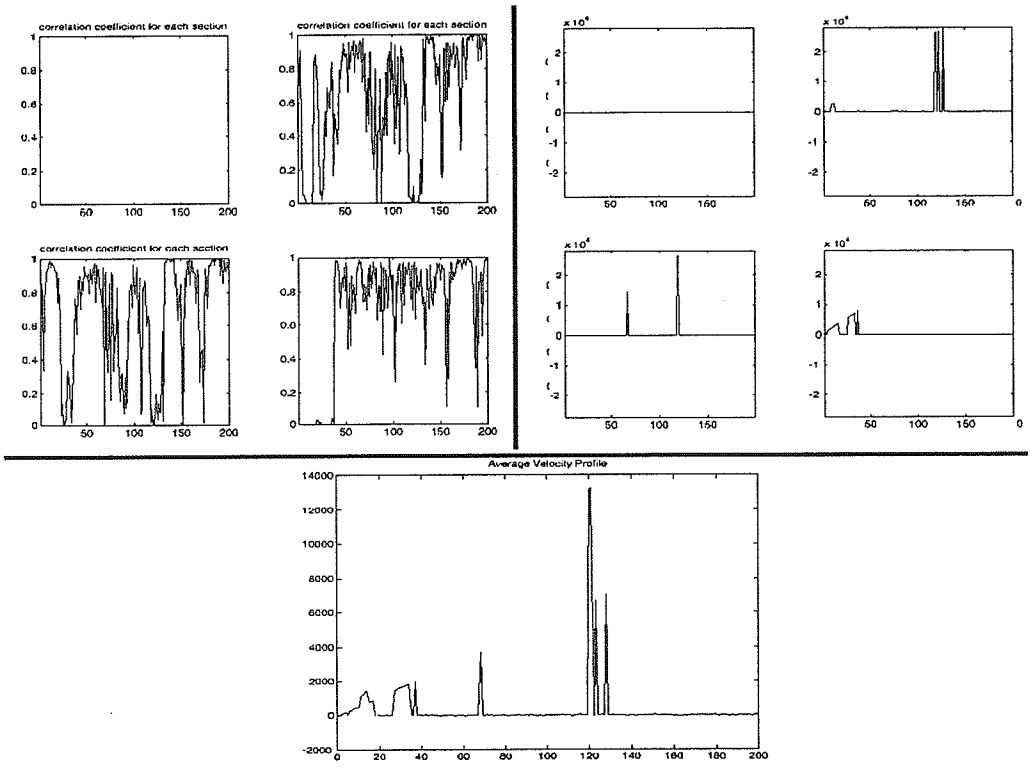


Figure 43. Guinea pig blood flow data-correlation and velocity profiles and averaged wave from the vena cava.

left by 15 pixels. The velocity curves do not indicate a parabolic shape as should be expected. Instead there is a strange effect of increasing shift from the left side to the right and only at few select points. It actually does look like a flow profile but it cannot be determined as to what this represents. These results took two days to generate on a Sparc 20 Sun workstation.

Figures 44, 45, and 46 represent the correlation results from the kidney data set. As can be seen from the averaged wave, there is no movement detected by the program except for a spike on one out of the six correlations. This indicates a total lack of flow in the organ (which is a real possibility) or some other cause such as inability of the program to detect flow. This is unlikely since all the velocity profiles remarkably are at zero. The most likely explanation is that there was no flow at the location or that it was too slow to be detected.

The flow results from the guinea pig are mixed and need to be further explored for their significance.

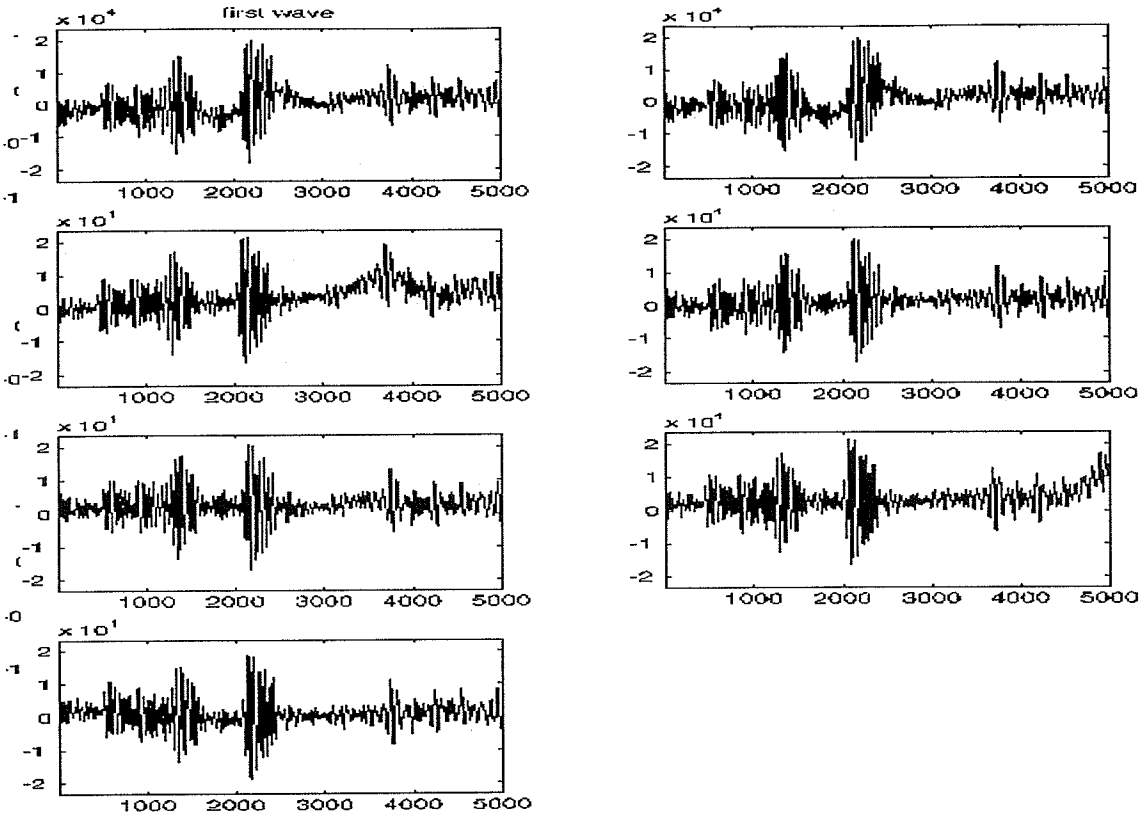


Figure 44. Guinea pig blood flow data-kidney waves.

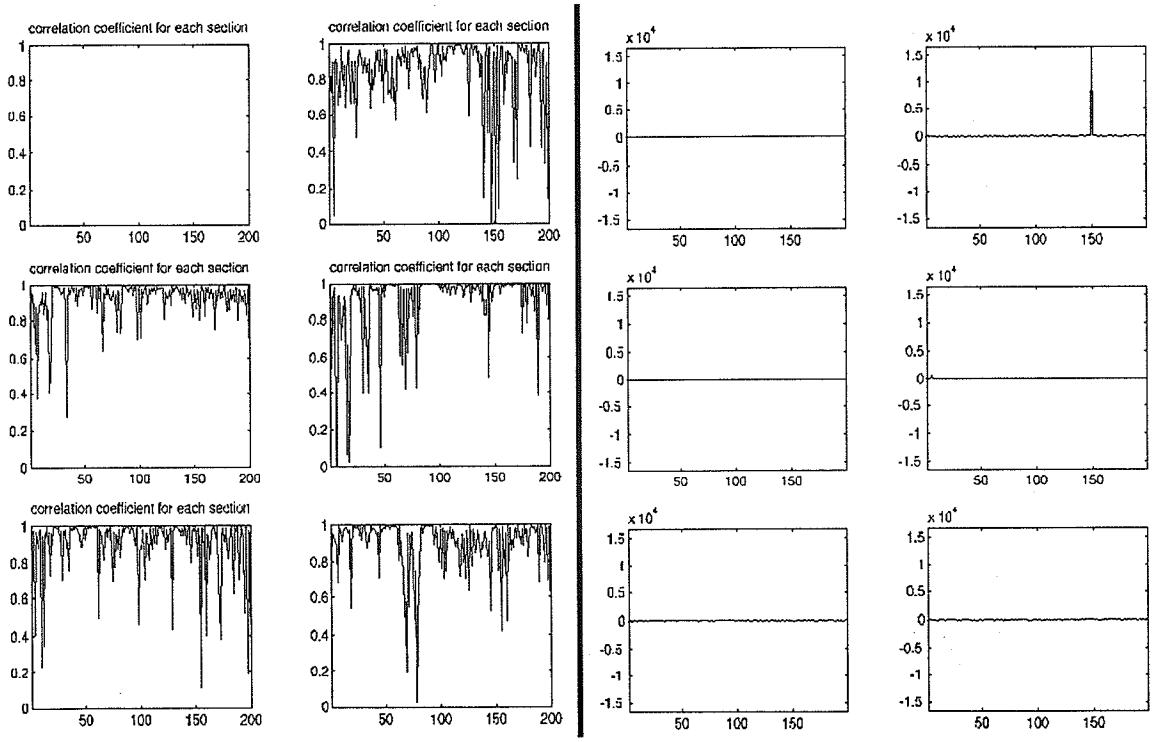


Figure 45. Guinea pig blood flow data-correlation and velocity profiles from the kidney.

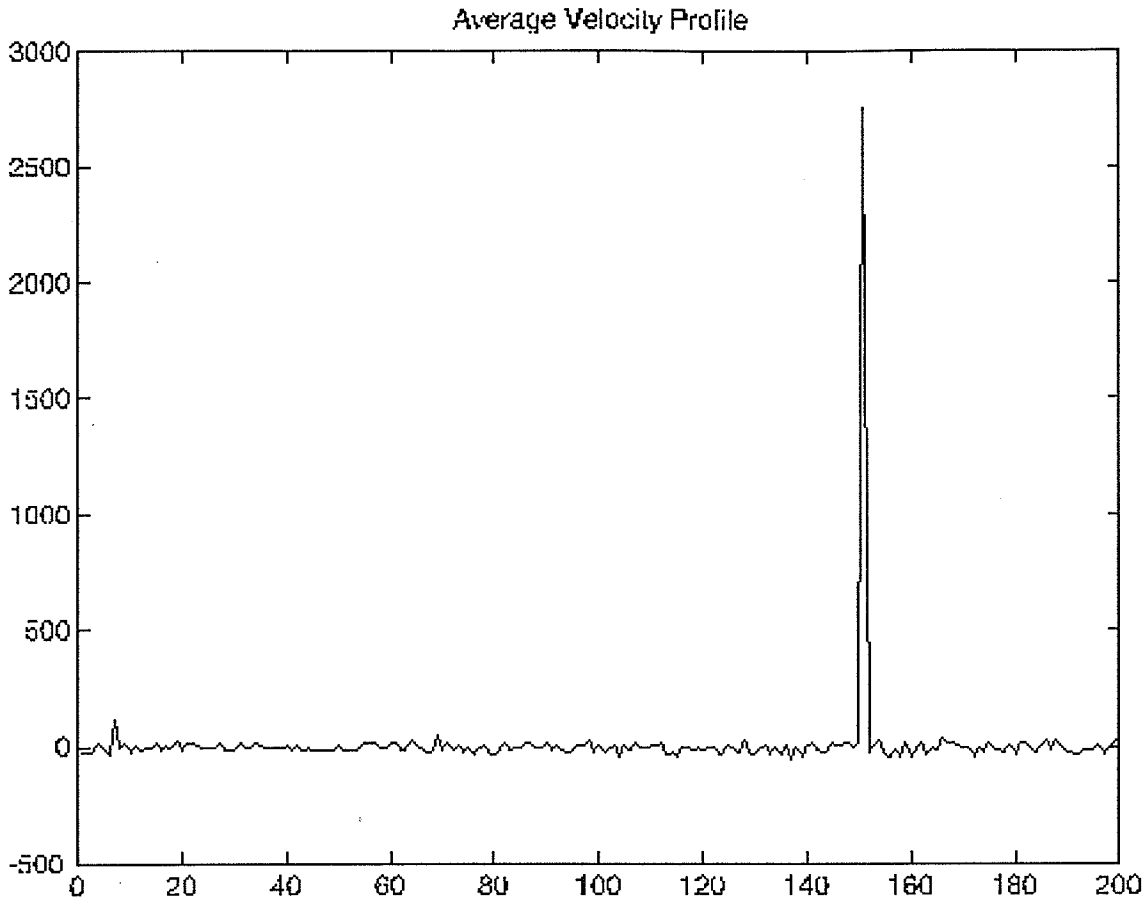


Figure 46. Guinea pig blood flow data-averaged wave from the kidney.

It is further used in a live guinea pig model to see if it can measure blood flow in various organs. B-mode images are taken of the liver, kidney, vena cava, and the stomach with a 20 MHz transducer. This is done in order to visualize the area being measured for flow. Flow profiles have been generated in the vena cava and the kidney. The results are inconclusive that the UTDC technique can measure blood flow in complex physiological conditions such as the flow in the kidney. The vena cava results need to be further explored. The flow profiles from the guinea pig do not confirm or deny the validity of this approach and further work needs to be done in the animal model to see if better measurement approaches can obtain clearer signals and thereby produce more accurate results.

# REFERENCES

[1] I. A. Hein, "Measurement of volumetric blood flow using ultrasound time domain correlation," Ph.D. dissertation, Dept. of Elec. Comput. Eng., Univ. Ill. at Urbana-Champaign, 1991.

[2] P. M. Embree and W. D. O'Brien, Jr., "Assessment of pulsed Doppler accuracy due to frequency-dependent attenuation and Rayleigh scattering error sources," IEEE Trans. Biomed. Eng., vol. 37, no. 3, pp. 322-326, March 1990.

[3] I. A. Hein and W. D. O'Brien, Jr., "Current time-domain methods for assessing tissue motion by analysis from reflected ultrasound echoes-A Review," IEEE Trans. Ultrason., Ferroelec., Freq., Contr., vol. 40, no. 2, pp.84-102, March 1993.

[4] P. M. Embree, "The accurate ultrasonic measurement of the volume flow of blood by the time domain correlation," Ph.D. dissertation, Dept. of Elec. Comput. Eng., Univ. Ill. at Urbana-Champaign, 1986.

[5] P.M. Embree and W.D. O'Brien, Jr., "Volumetric blood flow via time domain correlation: Experimental verification," IEEE Trans. Ultrason., Ferroelec., Freq., Contr., vol. 37, pp.176-189, May 1990.

[6] M. Bassini, D. Dotti, E. Gatti, P. L. Pizzolati, and V. Svelto, "An ultrasonic noninvasive blood flowmeter based on cross correlation techniques," Ultrason., Int., Proc., pp.273-278, 1979.

[7] S. G. Foster, P. M. Embree, and W. D. O'Brien, Jr., "Flow velocity profile via time domain correlation: error analysis and computer simulation," IEEE Trans. Ultrason., Ferroelec., Freq., Contr., vol. 37, pp.164-175, May 1990

[8] K. Ferrara, V. R. Algazi, and J. Liu, "The effect of frequency dependent scattering and attenuation on the estimation of blood velocity using ultrasound," IEEE Trans. Ultrason., Ferroelec., Freq., Contr., pp.754-767, Nov. 1992.

# APPENDIX

## CORRELATION COMPUTER PROGRAM

This appendix contains the Matlab code for the correlation program. Comments have been added where explanations are needed.

```
function
correlation(filename,numofpoints,numofscanstodo,everykthscan,pointsin1wave,timeperpo
intus,timebetweenwavesus,corr_resolution,maxsearchvel,radtheta,sections)

%Correlation Program that figures out velocity rates in cm/s of flow in a tube
%input variables:
%numofscanstodo=How many waves do you want to compare to the original
%filename= filename in single quotes ' ' of the filename-ascii format files
%pointsin1wave= # of points read from the Lecroy scope in one waveform(from the
%           timebase menu)
%timeperpointus=time for each point/pixel in us
%timebetweenwavesus=PRF of the signal
%corr_resolution=how many points are skipped in the next wave before another
%                   corellation is done
%maxserchvel=puts a limit on the number of pixels the program will search on
%          both side of the section
%radtheta= Doppler angle in radians-angle between transducer and the tube
%sections= How many sections do you want each wave divided into-higher the # of
%        sections, the higher the resolution of the flow profile



%Load the alldata file containing all the waves in consecutive order
%find the length and figure out how many there are

%use this for the Tektronix scope data
%fid=fopen(filename,'r');
%alldata=zeros(1:numofpoints);
%alldata=fread(fid('short'));
%fclose(fid);

%use this for the Lecroy scope data
fid=fopen(filename,'rb','l');
alldata=zeros(1:numofpoints);
alldata=fread(fid,numofpoints,'short');
fclose(fid);

%eval (['load ' ,filename]);
%alldata=eval(filename);
maxdata=max(alldata);
LENofalldata=length(alldata)
numofwaves=LENofalldata/pointsin1wave


%parse the alldata file into individual waves
```

```
for m=1:numofwaves
        suffix=int2str(m);
        for n=1:pointsin1wave
                setofdata(m,n)=alldata(n+(m-1)*pointsin1wave);
        end
end


%open all figures
figure(1);
figure(2);
figure(3);
figure(4);


%look at the first wave
xx=setofdata(1,:);
LL=length(xx);
sll=LL/sections;
figure(1);
orient tall;
subplot((numofscanstodo+2)/2,2,1),plot(xx);
axis([1 pointsin1wave -maxdata maxdata]);
title('first wave')


%temp is used to calculate velocity in CENTIMETRS/SECONDS
%timeperpointus is time per pixel/point in us of the wave
%152000 is the speed of sound in water in cm/s
%Period between adjacent waves is 'timebetweenwavesus' in us
%radtheta is the angle between the transducer and the tube
temp=(timeperpointus*150000)/(2*timebetweenwavesus*everykthscan*cos(radtheta));


%calculate the num of pixels that will be searched on both sides of a section
%depending on the maxsearchvel put in
numofsearchpixels=((2*timebetweenwavesus*everykthscan*cos(radtheta)*maxsearchvel)/
150000)/timeperpointus

%use this to override the above statement and set your own shift
%numofsearchpixels=100

%MAIN LOOP THAT DOES CORRRELATIONS AND VELOCITY
CALCULATION+PLOTTING
plotcounter=1;
for z=1:everykthscan:numofscanstodo*everykthscan


        %Divide the previous wave into origsections that are adjacent chopped up
        %sections
        xx=setofdata(z,:);
        for i=1:sections
                %origsection(i,1:sll)=zeros(1:sll);
           for j=1:sll
```

```
        origsection(i,j)=xx(j+(i-1)*sll);
    end
    %figure(5);
    %orient tall;
    %title('origsection');
    %subplot(sections/2,2,i),plot(origsection(i,1:sll));
    %axis([1 sll -maxdata maxdata]);
end


%Pick the next wave to work with and plot it
if z==1
        yy=setofdata(z,:);
else
        yy=setofdata(z+1,:);
end
L= length(yy);
sl=L/sections;
figure(1);
orient tall;
plotcounter=plotcounter+1;
subplot((numofscanstodo+2)/2,2,plotcounter),plot(yy);
axis([1 pointsin1wave -maxdata maxdata]);


%divide the next wave into sections that are sl long and differ from eac
%h other by being moved by a few("corr_resolution") pixels
for i=1:(L-sl)
        newsection(i,1:sl)=yy(i:i+sl-1);
end


%calculate corr coefficient and the velocity in cm/s for each section
for k=1:sections


    %figure out the exact number of pixels that the loop will search for
    a=round(sl*(k-1)-numofsearchpixels);
    if a<1  a=1; end
    if a>L  a=L; end
    b=round(sl*k+numofsearchpixels-sl);
    if b>L-sl  b=L-sl-1; end
    for i=a:corr_resolution:b
        R=xcorr(origsection(k,1:sl),newsection(i,1:sl),'coeff');
        sectionmaxcorrs(k,i)=max(R);
    end
    figure(4);
    orient tall;
    subplot(((sections+1)/2),2,k), plot(sectionmaxcorrs(k,:));
    axis([1 L 0 1]);
    title('section max corr');

    %pick out the max of the correlation coeffs for this section
```

```
            %and its location due to corr_resolution and find how much it has
            %moved(the sectionmaxcorrs vector is
            %(L-sl)/corr_resolution long
            [maxofsectionmaxcorrs(z,k),sectionmaxindex]=max(sectionmaxcorrs (k,:));
            origsectionmaxindex=sl/2+((k-1)*sl);
            distance_in_pixels=(origsectionmaxindex-sl/2-sectionmaxindex);
            velocity(z,k)=temp*distance_in_pixels;
        end


        %plot velocity and corr coeff
        figure(2);
        orient tall;
        title('vel (cm/s)');
        velmax=max(velocity(z,:));
        subplot((numofscanstodo+1)/2,2,plotcounter-1), plot(velocity(z,
                                                    2:sections-1));
        axis([1 sections -velmax velmax]);

        figure(3);
        orient tall;
        title('corr coeff');
        subplot((numofscanstodo+1)/2,2,plotcounter-1), plot(maxofsectionmaxcorrs
                                                        (z,1:sections));
        axis([1 sections 0 1]);
end


%plot scaled velocity and corr coeff
velmaxvector=max(velocity);
velmax2=max(velmaxvector);
plotcounter=0;
figure(2);
clf;
figure(3);
clf;

for i=1:sections
        avgvelocity(i)=0;
end
for z=1:everykthscan:everykthscan*numofscanstodo
        plotcounter=plotcounter+1;
        figure(2);
        orient tall;
        if z==1
                subplot((numofscanstodo+1)/2,2,plotcounter);
                title(['velocity(cm/s) ',filename]);
        end
        subplot((numofscanstodo+1)/2,2,plotcounter), plot(velocity(z,
                                            2:sections-1));
        axis([2 sections-1 -velmax2 velmax2]);

        for i=1:sections
                avgvelocity(i)=velocity(z,i)+avgvelocity(i);
```

```
        end

        figure(3);
        orient tall;
        if z==1
           subplot((numofscanstodo+1)/2,2,plotcounter);
           title(['velocity(cm/s) ',filename]);
      end
        title('correlation coefficient for each section');
        subplot((numofscanstodo+1)/2,2,plotcounter), plot(maxofsectionmaxcorrs
                                                    (z,1:sections));
        axis([1 sections 0 1]);

end

%Average the velocity profiles to get a single averaged profile
for i=1:sections
        avgvelocity(i)=avgvelocity(i)/numofscanstodo;
end
figure(5);
plot(avgvelocity);
title('Average Velocity Profile');
save (filename);
%save the variables and the velocity,corr coeff, waves figures
%saving=['save variables_', filename,'.mat ', 'velocity avgvelocity
maxofsection%maxcorrs everykthscan corr_resolution radtheta maxsearchvel
numofsearchpixels '%]
%eval ([saving]);
figure(1);
fig1=['print -dps ',filename,'_waves'];
eval([fig1]);
figure(2);
fig2=['print -dps ',filename,'_vel'];
eval([fig2]);
figure(3);
fig3=['print -dps ',filename,'_corr'];
eval([fig3]);
figure(5);
fig5=['print -dps ',filename,'_avgwave'];
eval([fig5]);

%have a nice day:)
```

# UNIVERSITY OF ILLINOIS AT URBANA-CHAMPAIGN

*GRADUATE COLLEGE DEPARTMENTAL FORMAT APPROVAL*

THIS IS TO CERTIFY THAT THE FORMAT AND QUALITY OF PRESENTATION OF THE THESIS SUBMITTED BY AMJAD ALI SAFVI AS ONE OF THE REQUIREMENTS FOR THE DEGREE OF MASTER OF SCIENCE ARE ACCEPTABLE TO THE DEPARTMENT OF ELECTRICAL AND COMPUTER ENGINEERING.

June 28 1996
*Date of Approval*

*Departmental Representative*